2018년 8월
석사학위 논문

# MWCNT/$Fe_3O_4$ 하이브리드 나노유체에서 열전도 및 광-열 변환 성능에 미치는 자기장 효과

조선대학교 대학원

기 계 공 학 과

척트빌렉트 벌더

# MWCNT/$Fe_3O_4$ 하이브리드 나노유체에서 열전도 및 광-열 변환 성능에 미치는 자기장 효과

Magnetic effect on thermal conductivity and photo-thermal conversion performance of MWCNT/$Fe_3O_4$ hybrid nanofluid

2019년 5월

조선학교 대학원

기 계 공 학 과

척트빌렉트 벌더

# MWCNT/$Fe_3O_4$ 하이브리드 나노유체에서 열전도 및 광-열 변환 성능에 미치는 자기장 효과

지도교수 : 조 홍 현

이 논문을 공학석사 학위신청 논문으로 제출함

2019년 5월

조선대학교 대학원

기 계 공 학 과

척트빌렉트 벌더

# 척트빌렉트 벌더의 석사학위 논문을 인준함

위원장 조선대학교 교수 오 동 욱 ㊞
위 원 조선대학교 교수 박 정 수 ㊞
위 원 조선대학교 교수 조 홍 현 ㊞

2019년 5월

# 조선대학교 대학원

# Contents

Contents ····· i
List of Figures ····· iii
List of Tables ····· vi
Nomenclature ····· vii
ABSTRACT ····· ix

Ⅰ. Introduction ····· 11
1.1 Background ····· 11
1.2 Previous studies ····· 13
1.3 Objectives ····· 21

Ⅱ. Experimental setup and method ····· 22
2.1 $Fe_3O_4$ nanoparticle synthesis ····· 22
2.2 Preparation of nanofluid ····· 24
2.3 Experimental setup of thermal conductivity test ···· 31
2.4 Experimental setup of optical transmittance test ···· 35
2.5 Experimental setup of photo-thermal conversion test ····· 39

Ⅲ. Results and discussion ····· 43
3.1 Optical result of $Fe_3O_4$, MWCNT, and MWCNT/$Fe_3O_4$ hybrid nanofluid ····· 43
3.2 Thermal conductivity of $Fe_3O_4$, MWCNT, and

MWCNT/$Fe_3O_4$ hybrid nanofluid ····· 51
3.3 Thermal conductivity of $Fe_3O_4$ nanofluid under an external magnetic field ····· 56
3.4 Thermal conductivity of MWCNT/$Fe_3O_4$ hybrid nanofluid under an external magnetic field ····· 62
3.5 Photo-thermal conversion performance of $Fe_3O_4$ nanofluid ····· 68
3.6 Magnetic effect on photo-thermal conversion performance of MWCNT/$Fe_3O_4$ hybrid nanofluid ····· 73

Ⅳ Conclusion ····· 80

REFERENCE ····· 82

# List of Figures

Fig. 1.1 Nanoscale ····· 12

Fig. 2.1 Co-precipitation manufacturing method of $Fe_3O_4$ nanoparticle ····· 23

Fig. 2.2 Basic principle of two-step nanofluid manufacturing method ····· 25

Fig. 2.3 Pictures of (a) $Fe_3O_4$, (b) MWCNT, and (c) MWCNT/$Fe_3O_4$ hybrid nanofluid ····· 27

Fig. 2.4 TEM image of (a) $Fe_3O_4$, (b) MWCNT, and (c) MWCNT/$Fe_3O_4$ hybrid nanofluid ····· 28

Fig. 2.5 Schematics and picture of thermal conductivity experimental setup ····· 33

Fig. 2.6 KD2-Pro thermal conductivity measurement device ····· 34

Fig. 2.7 Schematics and picture of light transmittance experimental setup ····· 37

Fig. 2.8 Avantes optical experiment device ····· 38

Fig. 2.9 Schematics of photo-thermal conversion experimental setup ····· 41

Fig. 2.10 Picture of (a) CR-110 irradiation transmitter and (b) K-type thermo couple ····· 42

Fig. 3.1 Variation of optical transmittance of (a) $Fe_3O_4$, (b) MWCNT, and (c) MWCNT/$Fe_3O_4$ hybrid nanofluid ····· 47

Fig. 3.2 Variation of solar weighted absorption fraction of $Fe_3O_4$ nanofluid with different weight concentration ····· 48

Fig. 3.3 Variation of solar weighted absorption fraction of MWCNT nanofluid with different weight concentration ····· 49

Fig. 3.4 Variation of solar weighted absorption fraction of MWCNT/$Fe_3O_4$ hybrid

nanofluid with different weight concentration ····· 50

Fig. 3.5 Variation of thermal conductivity with temperature at different weight concentrations of $Fe_3O_4$ nanofluid ····· 53

Fig. 3.6 Variation of thermal conductivity with temperature at different weight concentrations of MWCNT nanofluid ····· 54

Fig. 3.7 Variation of thermal conductivity with temperature at different weight concentrations of MWCNT/$Fe_3O_4$ hybrid nanofluid ····· 55

Fig. 3.8 Thermal conductivity variation of 0.005wt% $Fe_3O_4$ nanofluid under an external magnetic field ····· 59

Fig. 3.9 Thermal conductivity variation of 0.05wt% $Fe_3O_4$ nanofluid under an external magnetic field ····· 60

Fig. 3.10 Thermal conductivity variation of 0.2wt% $Fe_3O_4$ nanofluid under an external magnetic field ····· 61

Fig. 3.11 Thermal conductivity variation of 0.005wt% MWCNT/$Fe_3O_4$ hybrid nanofluid under an external magnetic field ····· 65

Fig. 3.12 Thermal conductivity variation of 0.05wt% MWCNT/$Fe_3O_4$ hybrid nanofluid under an external magnetic field ····· 66

Fig. 3.13 Thermal conductivity variation of 0.2wt% MWCNT/$Fe_3O_4$ hybrid nanofluid under an external magnetic field ····· 67

Fig. 3.14 Variation of temperature with the time for $Fe_3O_4$ nanofluid ····· 70

Fig. 3.15 Variation of temperature with the time for MWCNT nanofluid ····· 71

Fig. 3.16 Variation of temperature with the time for MWCNT/$Fe_3O_4$ hybrid nanofluid ····· 72

Fig. 3.17 Variation of temperature with the time for 0.2wt% MWCNT/$Fe_3O_4$ hybrid nanofluid under different magnetic intensity ····· 76

Fig. 3.18 Schematic of $Fe_3O_4$ nanoparticles under magnetic field ·····77

Fig. 3.19 Photo-thermal conversion efficiency of MWCNT/$Fe_3O_4$ hybrid nanofluid with different magnetic intensities ····· 78

Fig. 3.20 Total stored energy in 0.2wt% MWCNT/$Fe_3O_4$ hybrid nanofluid during the heating process with different magnetic intensities ·····79

# List of Tables

Table 1.1 Summary of reprehensive research about hybrid nanofluid ····· 15

Table 2.1 Physical properties of MWCNT and $Fe_3O_4$ nanoparticles ····· 29

Table 2.2 Physical properties of base fluid (20wt% EG/DI water) ····· 30

Table 2.3 Accuracy of KD2-Pro measurement device ····· 34

Table 2.4 Accuracy of Avantes measurement device ····· 38

Table 2.5 Accuracy of photo-thermal conversion measurement device ····· 42

# Nomenclature

| | |
|---|---|
| $A_m$ | : Solar weighted absorption fraction |
| A | : Area, $m^2$ |
| c | : Specific heat, J/kg°C |
| DASC | : Direct absorption solar collector |
| $E_{total}$ | : Total stored energy, kJ |
| e | : Euler's number |
| EG | : Ethylene glycol |
| F-MWCNT | : Functionalized MWCNT |
| G | : Heat flux of incident solar, $W/m^2$ |
| $k(\lambda)$ | : Extinction coefficient |
| K | : Thermal conductivity, W/mK |
| m | : Mass, g |
| MWCNT | : Multi-walled carbon nanotube |
| Q | : Heat rate, $W/m^2$ |
| $S_m$ | : Solar spectral irradiance in the atmosphere |
| $T(\lambda)$ | : Light transmittance |
| T | : Temperature, °C |
| t | : Time, s |
| w | : Weight, g |
| y | : Material thickness, mm |

## Greeks

| | |
|---|---|
| $\eta$ | : Efficiency |
| $\phi$ | : Weight concentration of nanofluid, wt% |
| $\rho$ | : Density |

## Subscript

| | |
|---|---|
| ave | : Average |
| bf | : base fluid |
| i | : Initial |
| max | : Maximum |
| min | : Minimum |
| nf | : Nanofluid |
| np | : Nanoparticle |

# Abstract

## Magnetic effect on thermal conductivity and photo-thermal conversion performance of MWCNT/$Fe_3O_4$ hybrid nanofluid

Tsogtbilegt Boldoo
Advisor: Prof. Honghyun Cho, PhD.
Graduate School of Chosun University

Due to the unregulated consumption of fossil resources, environmental pollution and catastrophic disasters were frequently occurred in the last decades. As a result, humankind has to harvest clean energy which does not emit greenhouse gases and toxic pollutions. Among the clean energy technologies, the solar collector is considered as the most efficient way to harvest thermal energy. Recently, many researchers have developed new working fluid in the solar collector, and it is called nanofluid that dispersed nano-sized materials into the base fluid such as water, ethylene glycol, thermal oil. Nanofluid can enhance the heat transfer efficiency of the solar collector, therefore it can reduce the size of solar collector.

In this study, photo-thermal conversion performance and thermal characteristics of MWCNT/$Fe_3O_4$ hybrid nanofluid suspended in water-ethylene glycol (20wt%), were experimentally investigated in the absence and presence of an external magnetic field. MWCNT/$Fe_3O_4$ hybrid nanofluid was prepared by various weight concentrations (0.005, 0.05, 0.2wt%) using a two-step method. The effect of

magnetic field on the photo-thermal conversion performance and thermal properties of MWCNT/$Fe_3O_4$ hybrid nanofluid was investigated under various magnetic intensities such as 250, 500, and 750 Gauss.

The experimental result shows that adding the MWCNT nanoparticles into the $Fe_3O_4$ nanofluid can achieve higher thermal properties of $Fe_3O_4$ nanofluid. The thermal conductivity of $Fe_3O_4$, MWCNT, and MWCNT/$Fe_3O_4$ hybrid nanofluid increased with the increase of temperature and weight concentration. The maximum thermal conductivity of $Fe_3O_4$, MWCNT, and MWCNT/$Fe_3O_4$ hybrid nanofluid were 0.562, 0.58, and 0.569 W/mK, respectively, at concentration and temperature of 0.2wt% and 50°C without an external magnetic field. In addition, the thermal conductivity of $Fe_3O_4$ and MWCNT/$Fe_3O_4$ hybrid nanofluid increased with the increase of magnetic field intensity. The maximum thermal conductivity of $Fe_3O_4$ and MWCNT/$Fe_3O_4$ hybrid nanofluid was 0.583 and 0.59 W/mK with the magnetic intensity of 750 Gauss, respectively. These were 4.69% and 4.73% enhanced, compared to those of without the external magnetic field.

Optical test results revealed that solar weighted absorption fraction of $Fe_3O_4$, MWCNT, and MWCNT/$Fe_3O_4$ hybrid nanofluid increased with the increase of weight concentration and penetration distance. MWCNT/$Fe_3O_4$ hybrid nanofluid increased significantly the solar weighted absorption fraction compared to that of $Fe_3O_4$ nanofluid. Moreover, photo-thermal conversion of $Fe_3O_4$, MWCNT, and MWCNT/$Fe_3O_4$ hybrid nanofluid increased with the weight concentration and operating time. In the presence of external magnetic field, 0.2wt% MWCNT/$Fe_3O_4$ hybrid nanofluid exhibited significant photo-thermal conversion enhancement, which was about 33% compared to that of 0.2wt% MWCNT/$Fe_3O_4$ hybrid nanofluid without the external magnetic field.

# I. Introduction

## 1.1 Background

A nanofluid has been widely investigated for various applications, since the innovation of the nanofluid in 1996 by Choi et al. [1]. A nanofluid is a heat transfer working fluid that containing nano-sized (10-100 nm) materials such as metal oxides, carbon materials, usually substances with favorable properties. In the micrometer scale, materials mostly perform the thermal and electric properties of the same bulk form of material; however, materials in the nano-scale may present different thermal and electric properties from that of bulk materials. In this range of nanoscale, the quantum effects rule the behavior and properties of particles. Generally, properties of materials are size-dependent in this nanoscale range. Moreover, properties such as melting point, optical, electrical conductivity, magnetic permeability, thermal properties, and chemical reactivity can be changed with the particle size in the nanoscale. According to the Maaz et al. [2], electrons in material cannot move freely and become restricted in nanoscale. This electron incarceration leads materials to behave to light differently. For example, gold will occur radiant yellow color at the macro-scale in bulk form, however in nanoscale, gold particles show red color. In nanoscale, melting point of gold decreases about 100°C with the decrease of diameter from 100 to 10 nm. Furthermore, when particle diameter of gold decreases less than 10 nm, the gold cannot conduct electric current. One of the beneficial concept at nanoscale is “tunability” of properties, which means that researchers can control a property of nanoparticle

by changing its shape and size.

Nanoscale materials have greater surface areas than similar masses of bulk materials. As specific surface area of a material increases, a larger amount of the fluid can come into contact with surrounding fluid, hence affecting thermal properties. The key parameters of nanoparticles are its shape, size, and structure of the substance as well as dispersion stability. In order to have a good dispersion stability, the surface and interfacial properties can be changed by surfactants. The particle-particle interactions are ruled by Van der Waals forces, stronger polar and electrostatic interactions or covalent interactions at the nanoscale. Fig. 1.1 shows the scale from macro to nano size.

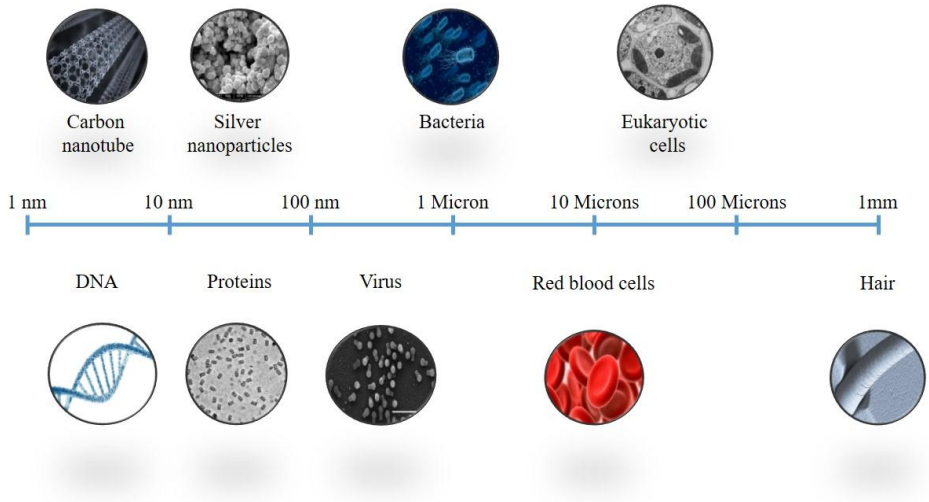


Fig. 1.1 Nanoscale

## 1.2 Previous studies

The main factors affecting the heat transfer efficiency of thermal system are the thermal and optical properties of working fluid. Nanofluids can enhance the heat-transfer efficiency of a heat exchanger and therefore it can reduce the size of the heat exchanger. Generally, nanoparticles have a high thermal conductivity, which improves the thermal conductivity and heat transfer of the working fluids z[3–9]. Furthermore, Gorji et al. [10] investigated the low flux DASC (direct absorption solar collector) using graphite, magnetite, and silver nanofluids. Their experimental results showed that outlet temperature of DASC improved by using nanofluid and increase of nanofluid concentration enhanced the higher outlet temperature at constant flow rate and solar heat flux. Moreover, the exergy efficiency of DASC was directly and reversely related with the solar radiation and flow rate.

Lately, synthesis, preparation, characterization and application of hybrid nanofluid were studied extensively in nanotechnology research communities. Usually, hybrid nanofluid manufactured by two or more nanoparticles homogeneously dispersed in conventional working fluid such as water, thermal oil, anti-freeze etc. Accordingly, using the compatible nanoparticles for the hybrid nanofluid has a fundamental assumption of achieving an enhancement in the thermal properties, which can make a highly efficient working fluid. Many experimental and numerical literatures presented that wide range of nanoparticles such as Ag, Al, Au, Carbon nanotubes (CNT), Cu, Fe, Graphite, Nano-Diamond (ND), Ni, Mg, Sn, Si, Ti, Zi, etc., and metal oxides were used. Table 1.1 shows a

summary of reprehensive research about the properties of hybrid nanofluids [11-18].

Nanofluids have some crucial applications including: Biomedical applications, drug delivery, cancer therapy, power plant heating and cooling, and heat exchanger system etc. The minor problem with the single nanofluid is either they have a good thermal property or better rheological properties. Single nanoparticles cannot have all beneficial properties necessary for a specific application. In practical use, some of the properties of single nanofluid does not have thermal and usable properties for sophisticated applications.

As shown in Table 1.1, the main concept of hybrid nanofluid is to achieve a high enhancement in thermophysical, hydrodynamic and heat transfer properties compared to single nanofluid. For example, the metal oxide like $Fe_3O_4$ presents unique properties in external electromagnetic field, but they show lower thermal conductivity and photo-thermal conversion performance compared to carbon materials such as graphene oxide and carbon nanotubes. By adding Multi-walled carbon nanotube (MWCNT) into $Fe_3O_4$ nanofluid may can reach superior thermal and optical properties simultaneously, and enhance the efficiency of the thermal system under external magnetic field. In particular, $Fe_3O_4$ nanoparticles attached to a MWCNT hybrid nanofluid has a reasonable chance of working in an adjustable magnetic field in order to improve the thermal performance.

Table 1.1 Summary of reprehensive research about hybrid nanofluid

| Researcher | Type | Important findings |
|---|---|---|
| Asadi et al. [11] | $Al_2O_3$/CNT | The thermal conductivity of the nanofluid is dependent on the stability of the hybrid nanoparticles in the nanofluid; enhancement of the thermal conductivity can reach 14.75% at a volume fraction of 0.01 for a gum Arabic(GA)-based nanofluid. |
| Sureshka et al. [12] | $Al_2O_3$/Cu | Maximum thermal conductivity of $Al_2O_3$/Cu hybrid nanofluid increment was 12.11% at 2vol%. |
| Parsian et al. [13] | $Al_2O_3$/Cu | Thermal conductivity enhancement of nanofluid at a higher solid volume fraction is more than that at a lower solid volume fraction. A maximum thermal conductivity of 28% was observed at 50°C and 2vol%. |
| Dalkilic et al. [14] | CNT/$SiO_2$ | According to the enhancement properties, water-based CNT-$SiO_2$ hybrid nanofluid was recommended for heat transfer fluid at volume fractions higher than 1%. |
| Akhgar et al. [15] | CNT/$TiO_2$ | Increment in the volume fraction was found to increase thermal conductivity more effectively than temperature, the thermal conductivity of nanofluid can increase by a maximum of 38.7%. |

| | | |
|---|---|---|
| Trinh et al. [16] | Gr/CNT | The nanofluid containing 0.07vol% Gr-CNT hybrid material showed a thermal conductivity enhancement of 18% and 50% at 30°C and 50°C, respectively. These values are much higher in comparison with nanofluid containing only single-phase CNT or Gr. |
| Aberoumand et al. [17] | Ag/$WO_3$ | The results showed that the thermal conductivity of hybrid nanofluid increased by 41% in higher weight fraction at 100°C. Finally, it was observed that the electrical conductivity of hybrid nanofluid decreased to 35 kV in 4wt%. |
| Esfe et al. [18] | MgO/CNT | At a constant volume fraction, adding a specified amount of nanoparticles into the nanofluid at a high temperature is less effective on the thermal conductivity than at low temperatures. |

Karami et al. [19] reported that exergy efficiency increases with the mass flow rate and concentration of nanofluid in he DASC system by using $Fe_3O_4/SiO_2$. They showed that the entropy generation decreased when concentration of nanofluid and mass flow rate were decreased. Also, Bejan number showed that contribution of pressure drop the entropy generation were negligible. According to the DASC efficiency improvement by using $CeO_2$/CuO hybrid nanofluid [20], the efficiency of DASC was heavily dependent on the concentration of $CeO_2$ nanoparticle in hybrid nanofluid, and they concluded that efficiency of DASC using hybrid nanofluid were mainly dependent on concentration of nanoparticle that has a superior thermal property. Bhalla et al. [21] studied that photo-thermal conversion and solar weighted absorption fraction of $Al_2O_3/Co_3O_4$ hybrid nanofluid. They reported that solar weighted absorption fraction of $Al_2O_3/Co_3O_4$ hybrid nanofluid could absorb more than 80% of solar radiation for a penetration depth of 20 mm. $Fe_3O_4$/multi-walled CNT (MWCNT) combinations have rarely been reported in the open literature. In particular, $Fe_3O_4$ nanoparticles attached to an MWCNT hybrid nanofluid have a reasonable chance to improve the thermal performance under an adjustable magnetic field.

Compared with other nanoparticles, MWCNTs have a higher thermal conductivity and greater light absorption. In the study of Liu et al. [22], MWCNT nanoparticles suspended in EG/water exhibited a significant thermal conductivity enhancement which was nearly 30%. Furthermore, Qu et al. [23] investigated the photo-thermal conversion characteristics of an MWCNT nanofluid. Their experimental results indicated that the photo-thermal efficiency of the 0.01wt% MWCNT nanofluid was 32.5% higher than that of the water after 45 min under light irradiation. Abreu et al. [24] investigated the convective heat transfer of an MWCNT nanofluid and

reported a 47% enhancement of the convective heat transfer coefficient at a concentration of 0.5vol%. Additionally, a functionalized MWCNT (F-MWCNT) nanofluid exhibited better thermal properties than a non-functionalized MWCNT nanofluid, in the study of Soltanimehr et al. [25].

$Fe_3O_4$ has significant magnetic properties which can affect the thermal conductivity of the nanofluid. Karimi et al. [26] reported that a $Fe_3O_4$ nanofluid exhibited a 196% increase at a concentration of 4.8vol% under a magnetic field. Hajiyan et al. [27] found that the presence of a magnetic field significantly increased the viscosity and thermal conductivity of a $Fe_3O_4$ nanofluid. Additionally, the effect of the magnetic field was more pronounced for high volume fractions of the $Fe_3O_4$ nanofluid. In their study, the maximum enhancement ratio was 7.2 at a concentration of 3vol% under a 543 Gauss magnetic field. Sha et al. [28] compared the convective heat transfer performance of a $Fe_3O_4$ nanofluid in the absence of a magnetic field and reported that the maximum average enhancement of the convective heat transfer was 4.2% and 8.1% when uniform and gradient magnetic fields of 800 G were applied, respectively. To enhance the convective heat transfer of a $Fe_3O_4$ nanofluid, Amani et al. [29] used a porous metal foam tube under a magnetic field, which led to a 23.4% enhancement of the heat transfer at a concentration and magnetic field intensity of 2wt% and 200 Gauss, respectively. Sundar et al. [30] investigated the friction factor in a tube with a $Fe_3O_4$ nanofluid and found that the friction factor in a plain tube at 0.6vol% $Fe_3O_4$ nanofluid was enhanced by factors of 1.09 and 1.10 for Reynolds numbers of 3000 and 22000, respectively, compared with water.

$Fe_3O_4$ nanofluid can be used in various fields, such as water purification, seawater desalination, and distillation because $Fe_3O_4$ nanoparticles can be

separated from the fluid by using magnets after the heat transfer or water purification process. Shui et al. [31] used $Fe_3O_4$/CNT nanoparticles for high efficiency solar vapor generation. In their study, the $Fe_3O_4$/CNT nanoparticles were successfully separated from water after a purification process using magnets.

In the representative study on the properties of the MWCNT/$Fe_3O_4$ hybrid nanofluid, Sundar et al. [32] found that the thermal conductivity increased by 29% and the viscosity increased by a factor of 1.5 with 0.3wt% at 60℃ compared with the water. Harandi et al. [33] examined the effects of the temperature and concentration on the thermal conductivity of an F-MWCNT-$Fe_3O_4$/EG hybrid nanofluid. Their experimental results indicated that the maximum thermal conductivity enhancement was 30% at a temperature of 50℃ and a concentration of 2.3vol%. Additionally, they assumed that the ratio of the thermal conductivity enhancement to the solid volume fraction increased with the temperature. The numerical model of Mohebbi et al. [34] showed that adding MWCNT/$Fe_3O_4$ hybrid nanoparticle into water (working fluid) increased heat transfer rate in all their experimental cases. Shi et al. [35] investigated a $Fe_3O_4$/MWCNT hybrid nanofluid with controllable heat-transfer performance under a magnetic field. Their results suggested that the heat transfer of the $Fe_3O_4$/MWCNT hybrid nanofluid was mainly dependent on the magnetic force and direction.

The $Fe_3O_4$ nanofluid has great potential to enhance the thermal properties when it is used in the presence of a magnetic field; however, studies on the thermal properties of the $Fe_3O_4$ nanofluid are limited. Both Gupta et al. [36] and Babu et al. [37] made a review study on synthesis and thermophysical properties of hybrid nanofluids. They concluded that most of the published studies on hybrid nanofluid focused on thermal conductivity and viscosity whereas other properties such as

density, optical, specific heat, and photo-thermal properties are ignored. They deducted that huge hole remained for more dedicated and specific studies on applications of hybrid nanofluid. The $Fe_3O_4$ nanofluid has multiple applications apart from the convective heat transfer system. The main objective of the present study was to enhance the photo-thermal conversion property of the $Fe_3O_4$ nanofluid via the addition of MWCNT nanoparticles. Owing to their unique magnetic properties, $Fe_3O_4$ nanoparticles can be separated from the fluid and used for many other purposes. Moreover, previous studies revealed that MWCNT/$Fe_3O_4$ hybrid nanoparticles can be effectively separated from the fluid via magnets, because the $Fe_3O_4$ hybrid nanoparticles are attached to the MWCNT nanoparticles. With the exception of the thermal conductivity of MWCNTs, the effects of MWCNTs on hybrid nanofluids, such as the optical and photo-thermal conversion characteristics, have hardly been investigated. Moreover, adding MWCNTs to the $Fe_3O_4$ nanofluid can significantly affect its properties owing to the high thermal conductivity and absorption ability.

## 1.3 Objectives

The $Fe_3O_4$ nanofluid has a high potential to improve the thermal properties when it is used under the presence of a magnetic field, but some studies on the thermal properties of the $Fe_3O_4$ nanofluid are not sufficient and its theory was not established. Except from convective heat transfer applications, the $Fe_3O_4$ nanofluid can have a wide applications, for example sea water desalination, water distillation, and water purification etc. Moreover, there is a high potential that MWCNT/$Fe_3O_4$ hybrid nanofluid can be achieve efficient water purification system because after cleaning process MWCNT/$Fe_3O_4$ nanoparticles can be separated from fluid by using magnets, which can prevent secondly pollution in fluid.

The core purpose of this study is to improve the photo-thermal conversion property of $Fe_3O_4$ nanofluid with help of MWCNT nanoparticle under an external magnetic field. In this investigation, the magnetic effect on thermal conductivity and photo-thermal conversion performance of $Fe_3O_4$, MWCNT, and MWCNT/$Fe_3O_4$ hybrid nanofluid were analyzed based on experimental data, and experiments were carried out with $Fe_3O_4$, MWCNT and MWCNT/$Fe_3O_4$ hybrid nanofluid concentrations of 0.005wt%, 0.05wt%, 0.2wt%. In this study, the ethylene glycol and water mixture (weight ratio 20:80) used as a base fluid. In case of hybrid nanofluid, nanoparticle weight mixing ratio of $Fe_3O_4$ and MWCNT was fixed at 50:50. Moreover, the magnetic intensity of external magnetic field varied from 0 to 750 Gauss.

# Ⅱ. Experimental setup and method

## 2.1 $Fe_3O_4$ nanoparticle synthesis

In this experiment, co-precipitation method was used to synthesize the $Fe_3O_4$ nanoparticles. Ferrous chloride ($FeCl_2$) and iron (III) chloride ($FeCl_3$) were magnetically stirred in heating beaker at temperature of 50°C. During the stirring process, aqua ammonia solution ($NH_4OH$) was added drop by drop into the iron chloride mixture in heating beaker at temperature of 50°C. The chemical balance equation of synthesis process can be expressed as follows:

$$FeCl_2 + 2FeCl_3 + 8NH_4OH \Rightarrow Fe_3O_4 + 8NH_4Cl + 4H_2O \quad (1)$$

As adding aqua ammonia solution ($NH_4OH$), color of iron chloride mixture turned from yellow to dark brown. After that, $Fe_3O_4$ nanoparticles were separated from ammonium chloride ($NH_4Cl$) by magnets, and washed with diluted water at least 3 times. Thereafter, pure $Fe_3O_4$ nanoparticles were coated with aqueous poly(acrylic acid) solution at temperature of 90°C for 1 h. After coating process, the $Fe_3O_4$ and poly(acrylic acid) mixture was cooled until its temperature reaches to the room temperature and dried in a vacuum filter. Fig. 2.1 explained visually the whole synthesizing and coating process of $Fe_3O_4$ nanoparticle synthesis.

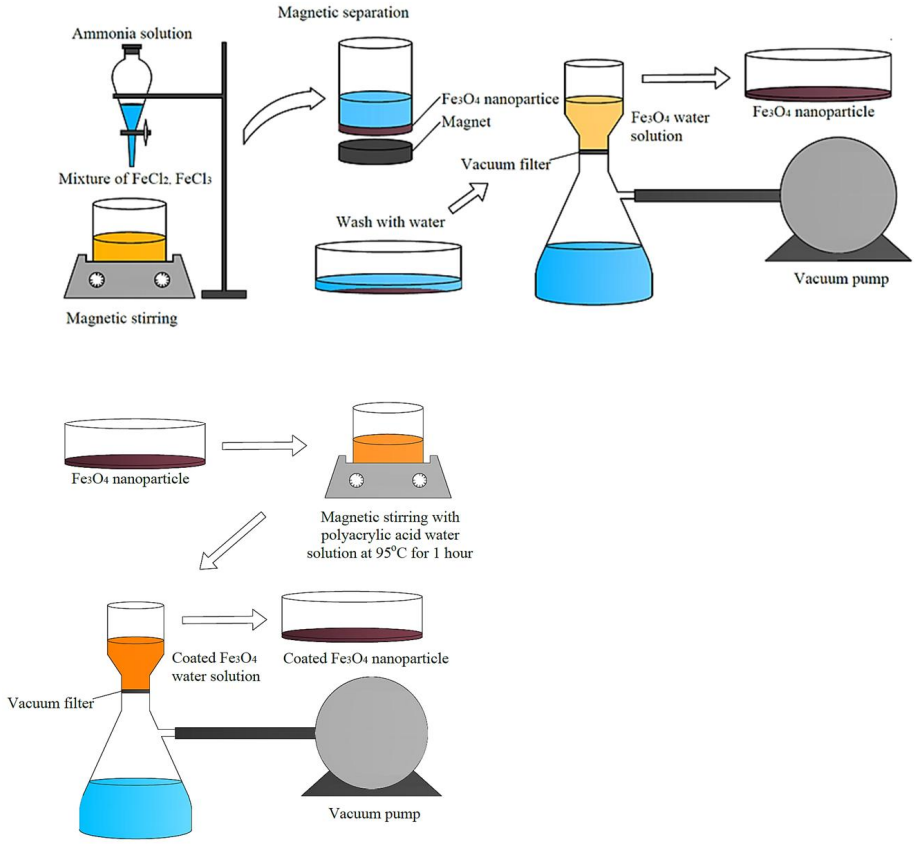


Fig. 2.1 Co-precipitation manufacturing method of $Fe_3O_4$ nanoparticle

## 2.2 Preparation of MWCNT/$Fe_3O_4$ hybrid nanofluid

In this experiment, $Fe_3O_4$ and MWCNT nanoparticles (US nano, Inc) were used to produce the $Fe_3O_4$, MWCNT and MWCNT/$Fe_3O_4$ hybrid nanofluid by a two-step manufacturing method, which is shown in Fig. 2.2. In order to disperse nanoparticles homogeneously, $Fe_3O_4$, MWCNT, and MWCNT/$Fe_3O_4$ nanoparticles was mixed in the ethylene glycol-water (weight ratio 20:80) solution by using ultrasonication processor for 2 h. The nanoparticle mixing ratio of MWCNT/$Fe_3O_4$ hybrid nanofluid was fixed at weight mixing ratio of 50:50, and also weight concentrations of $Fe_3O_4$, MWCNT, and MWCNT/$Fe_3O_4$ hybrid nanofluid were 0.005wt%, 0.05wt%, and 0.2wt%, respectively. The weight of nanoparticles was calculated by mass of base fluid as shown in Eq. (2):

$$m_{np} = \frac{\phi \cdot m_{bf}}{(100 - \phi)} \tag{2}$$

where $\phi$ is the weight concentration of nanofluid, $m_{bf}$ and $m_{np}$ are the mass of base fluid and nanoparticle. To disperse $Fe_3O_4$ nanoparticles in nanofluid uniformly, chemical agent poly(acrylic acid) was used to coat the surface of $Fe_3O_4$ nanoparticle. As shown in Fig. 2.3, $Fe_3O_4$, MWCNT and MWCNT/$Fe_3O_4$ hybrid nanofluid showed good dispersion stability, and also sedimentation was not observed during the experiments after multiple use. Moreover, color of nanofluid changed light to dark when concentration of nanofluid increased.

Fig. 2.4 shows the structural characterization of $Fe_3O_4$, MWCNT, and MWCNT/$Fe_3O_4$ nanoparticles in nanofluid by using transmission electron microscopy (TEM). In Fig. 2.4(a), the $Fe_3O_4$ nanoparticles dispersed well in nanofluid, and also Fig. 2.4(c) presented the shape of $Fe_3O_4$ nanoparticles attached to the MWCNT nanoparticles. The physical properties of $Fe_3O_4$, MWCNT nanoparticles and base fluid are given in Tables 2.1 and 2.2.

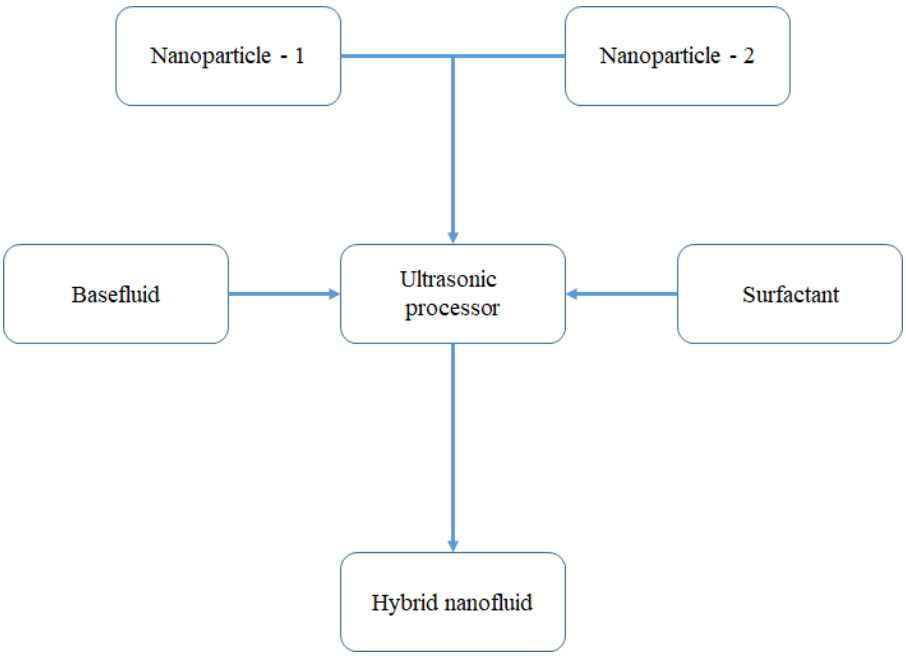


Fig. 2.2 Basic principle of two-step nanofluid manufacturing method

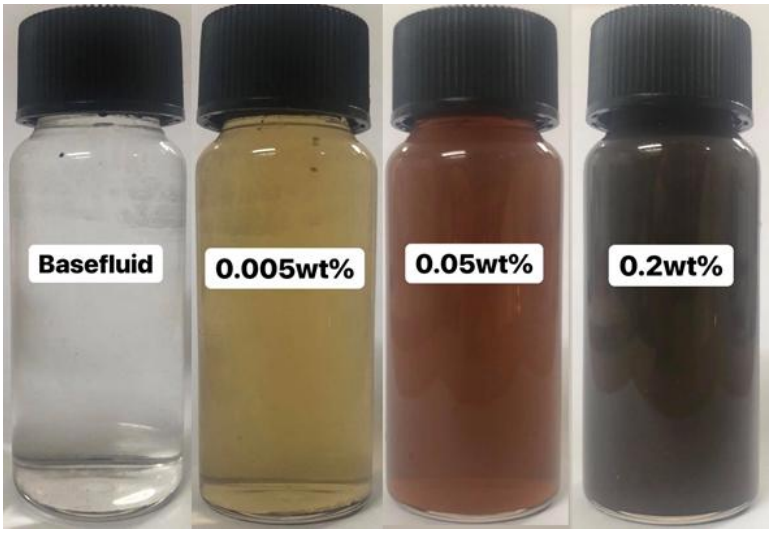


(a) $Fe_3O_4$ nanofluid

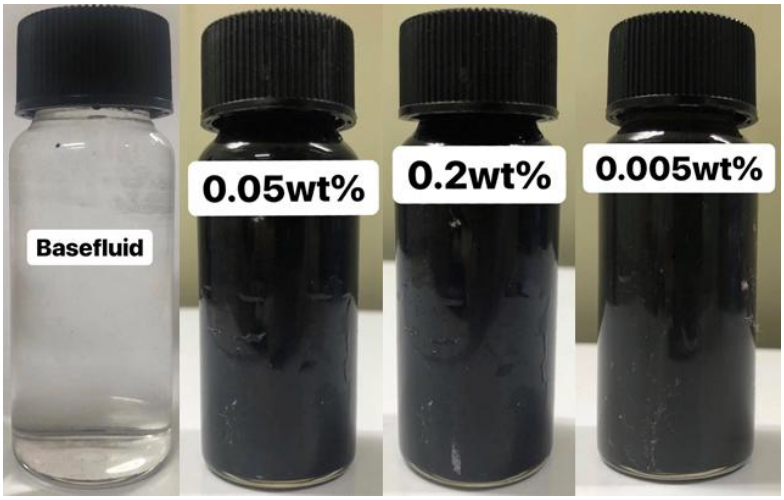


(b) MWCNT nanofluid

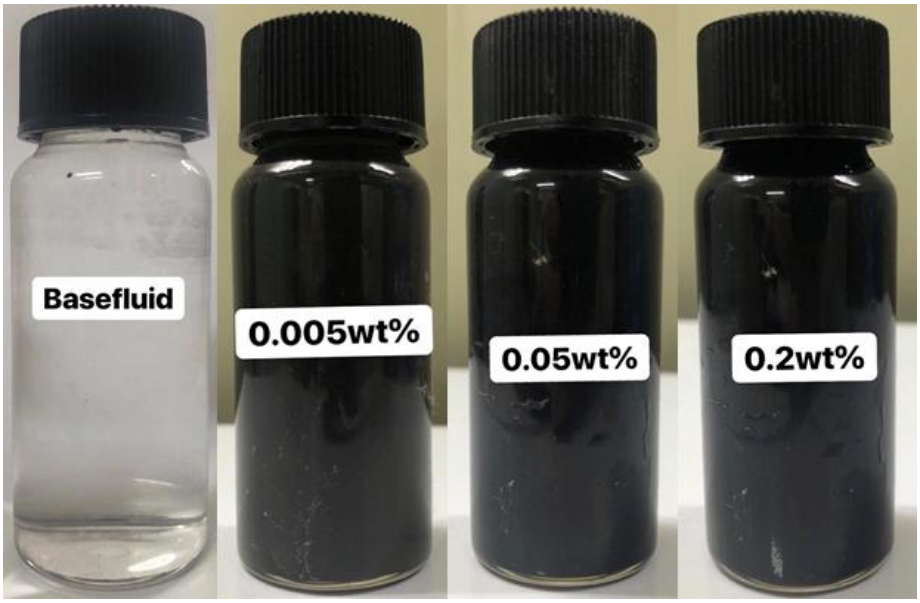


(c) MWCNT/$Fe_3O_4$ hybrid nanofluid

Fig. 2.3 Pictures of (a) $Fe_3O_4$, (b) MWCNT, and (c) MWCNT/$Fe_3O_4$ hybrid nanofluid

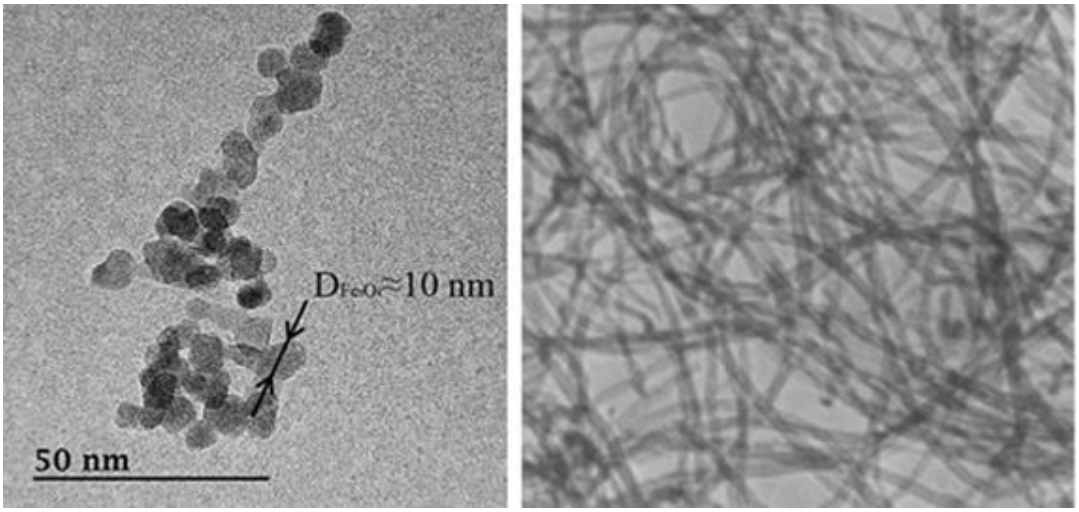


(a) $Fe_3O_4$ nanofluid (b) MWCNT nanofluid

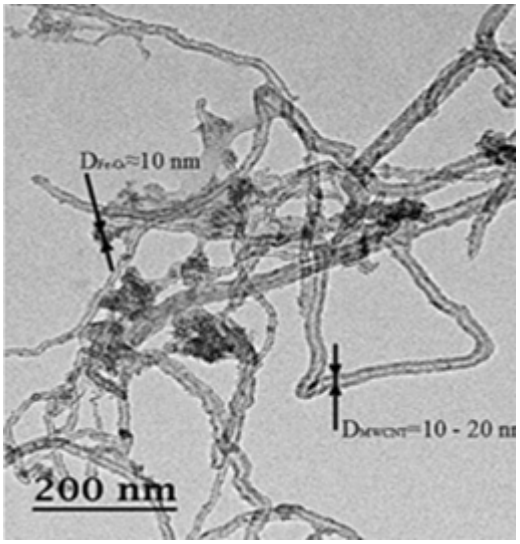


(c) MWCNT/$Fe_3O_4$ hybrid nanofluid

Fig. 2.4 TEM image of (a) $Fe_3O_4$, (b) MWCNT, and (c) MWCNT/$Fe_3O_4$ hybrid nanofluid

Table 2.1 Physical properties of MWCNT and $Fe_3O_4$ nanoparticles

| | MWCNT | $Fe_3O_4$ |
|---|---|---|
| Purity (%) | >95 | 99.5 |
| Color | Black | Dark brown |
| Outer diameter (nm) | 10-20 | 10 |
| Inner diameter (nm) | 5-10 | - |
| Length (μm) | 10-30 | - |
| Thermal conductivity (W/mK) | 1500 | 80 |
| True density ($g/cm^3$) | 2.1 | 5.1 |
| Manufacturing method | CVD | Co-precipitation |

Table 2.2 Physical properties of base fluid (20wt% EG/DI water)

| Temperature (°C) | Density ($kg/m^3$) | Viscosity ($m^2/s$) | Thermal conductivity (W/mK) |
|---|---|---|---|
| 20 | 1029.72 | 1.65 | 0.497 |
| 30 | 1026.02 | 1.3 | 0.509 |
| 40 | 1021.83 | 1.06 | 0.52 |
| 50 | 1017.16 | 0.88 | 0.529 |

## 2.3 Experimental setup of thermal conductivity test

Thermal conductivity is the most important property in a heat transfer system, and also thermal conductivity is a property of fundamental interest in developing the application of working fluids. The steady state hot wire experiment is one of the old and well established method. The hot wire system normally involves a vertical, cylindrical symmetry where the wire serves both as heating element and as thermometer. This method is classified by transient because the power is applied abruptly and the measurement is of short duration. In this experiment, KD2-Pro thermal properties analyzer (Decagon devices, Inc. USA) was used in this study. A probe of this measurement device consists of needle with a heater and temperature sensor. A electric current passes through the heater and the system monitors the temperature of sensor over time. The sensor needle is stainless steel KS-1 sensor with diameter and length of 1.3 and 60 mm. Before starting test, measurement device was calibrated by using water. Thermal conductivity of $Fe_3O_4$, MWCNT, and MWCNT/$Fe_3O_4$ hybrid nanofluid was measured at temperature ranging from 20°C to 50°C, under magnetic intensities of 250, 500, 750 Gauss. Schematics and picture of thermal conductivity experiment is shown in Fig. 2.5. Thermal conductivity of nanofluid was analyzed by following equation.

$$k = \frac{q(\ln t_2 - \ln t_1)}{4\pi(\triangle T_2 - \triangle T_1)} \tag{3}$$

where $q$ is constant heat rate, and $\triangle T_1$ and $\triangle T_2$ are the temperature changes

at times $\triangle t_1$ and $\triangle t_2$ respectively. In order to generate the external magnetic field, the electromagnetic generator and the magnetic measurement device, a custom made JLMAGNET generator (JLMagnet, South Korea) and a TM-801 EXP teslameter (Kanetec, Japan) were used, respectively. To confirm the results of measurement, all samples measured at leat 5 times in one condition. Accuracy and picture of thermal properties analyzer KD2-Pro are shown in Table 2.3 and Fig. 2.6.

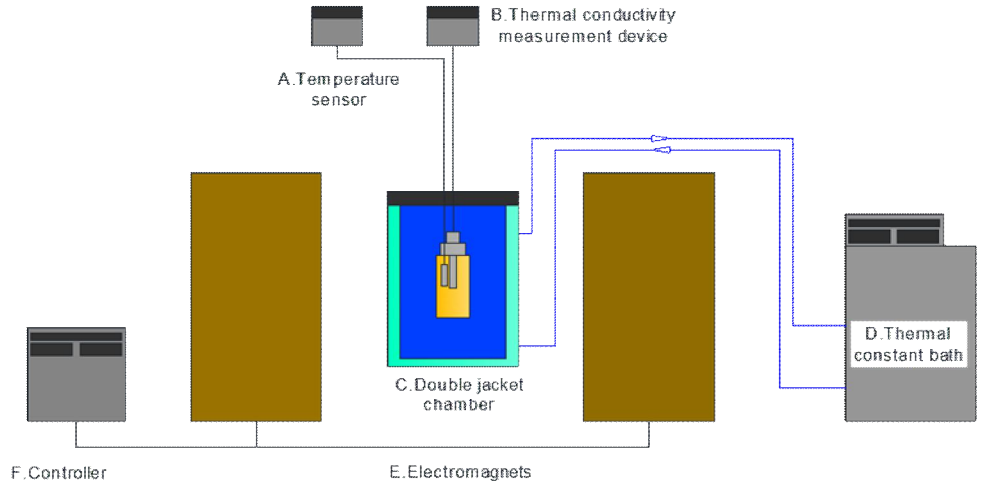


(a) Schematics of thermal conductivity experimental setup


(b) Picture of thermal conductivity experimental setup

Fig. 2.5 Schematics and picture of thermal conductivity experimental setup

Table 2.3 Accuracy of KD2-Pro measurement device

| Experiment | Model | Range | Accuracy |
|---|---|---|---|
| Thermal conductivity test | KD2-Pro | 0.02-2.00 W/mK | ±0.01 W/mK |


Fig. 2.6 KD2-Pro thermal conductivity measurement device

## 2.4 Experimental setup of optical transmittance test

In order to investigate the optical properties of $Fe_3O_4$, MWCNT, and MWCNT/$Fe_3O_4$ hybrid nanofluid, the AvaSpec-ULS2048 versatile fiber-optic spectrometer and AvaLight light source was used in the region of UV-VIS-NIR (300-1300 nm) at room temperature of 25°C. To confirm measurement data of each sample was measured at least 3 times in a quartz cuvette container with width of 10 mm. One of the main property in photo-thermal conversion system is solar weighted absorption fraction, which describes the fraction of the incident solar energy that could be absorbed by a given thickness of the fluid layer, which was calculated by Eq. (4).

$$A_m = \frac{\int_{300nm}^{1300nm} S_m (1 - e^{k(\lambda)x}) dx}{\int_{300nm}^{1300nm} S_m d\lambda} \tag{4}$$

where $S_m$ is solar spectral irradiance in the atmosphere, $k(\lambda)$ is extinction coefficient by wavelength, which can calculated by Beer-Lambert law [38]. as expressed in Eq. (5)

$$T(\lambda) = e^{-k(\lambda)_{e,\lambda} y} \tag{5}$$

where $T(\lambda)$ is light transmittance, $k_{e,y}$ is absorption efficiency, and y is material thickness (10 mm glass cuvette). The solar weighted absorption fraction

for different penetration distance is an important characteristic in the design of photo-thermal conversion application system because this provides information regarding the optimum mass fraction and the height of the collector system. Schematics and picture of light transmittance experimental setup are shown in a Fig. 2.7. Moreover, accuracy and picture of Avates measurement device are shown in Table 2.4 and Fig. 2.8, respectively.

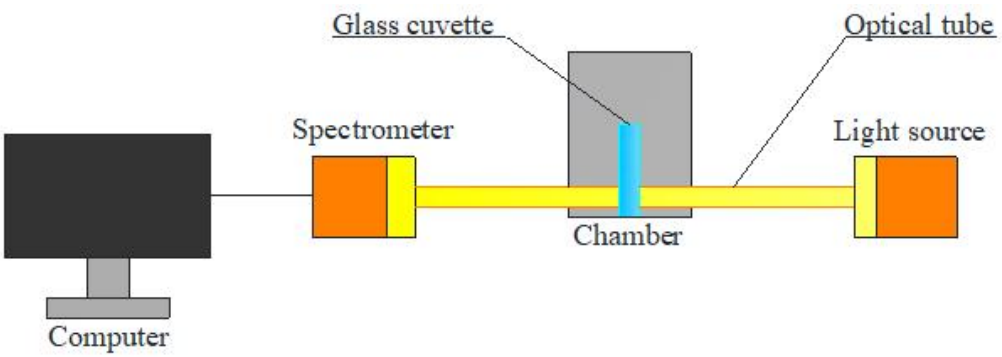


(a) Schematics of light transmittance experimental setup

(b) Picture of light transmittance experimental setup

Fig. 2.7 Schematics and picture of light transmittance experimental setup

Table 2.4 Accuracy of Avantes measurement device

| Experiment | Model | Range | Accuracy |
|---|---|---|---|
| Optical transmittance test | AvaSpec-2048 | 200-1300 nm | 0.04 - 20 nm |


Fig. 2.8 Avantes optical experiment device

## 2.5 Experimental setup of photo-thermal conversion test

A schematics of the experimental setup used to measure the photo-thermal conversion performance under external magnetic field is shown in Fig. 2.9. The sample beaker has the capacity of 40 ml, and located in the center of the external magnetic field. Also, prevent heat loss from sample to ambient air, extruded polystyrene (XPS) foam was used as a thermal insulation. The top side of the sample beaker was covered with the glass to absorb the solar energy as much as possible. Moreover, three K-type thermocouple was connected to the data acquisition system in different heights of sample beaker, and also recorded every 30 sec for 60 min, to precisely investigate the temperature gradient of the $Fe_3O_4$, MWCNT, and MWCNT/$Fe_3O_4$ hybrid nanofluid. Samples were irradiated by the light source, an 800 W solar simulator of Halogen light.

In order to generate the external magnetic field, electromagnetic generator and the magnetic measurement device, a custom made JLMAGNET generator (JLMagnet, South Korea) and a TM-801 EXP teslameter (Kanetec, Japan) were used, respectively. In the photo-thermal conversion test of the $Fe_3O_4$, MWCNT, and MWCNT/$Fe_3O_4$ hybrid nanofluids, the average ambient temperature and solar irradiance were set to approximately 20°C and 560 W/m$^2$, respectively. The photo-thermal conversion efficiency is given by Eq. (6).

$$\eta = \frac{mc_p(T_i - T_s)}{GA\Delta t} \tag{6}$$

Where $m$ and $c_p$ are the mass and specific heat of nanofluid, respectively, $T_i$

is the initial temperature of the nanofluid, $T_s$ is the instantaneous temperature, $A$ is the surface area of the cylinder cup, $G$ is the heat flux of the sun, and $\Delta t$ is the exposure time to solar radiation. Accuracy and picture of solar irradiation and thermocouple are shown in Table 2.5 and Fig. 2.10. The total stored energy in the working fluid under heating can be expressed by Eq. (7) [39].

$$E_{total} = m_f c_f (T_{\max} - T_{\min}) \tag{7}$$

where $T_{\max}$ and $T_{\min}$ represent the maximum and minimum temperature of the working fluid, respectively.

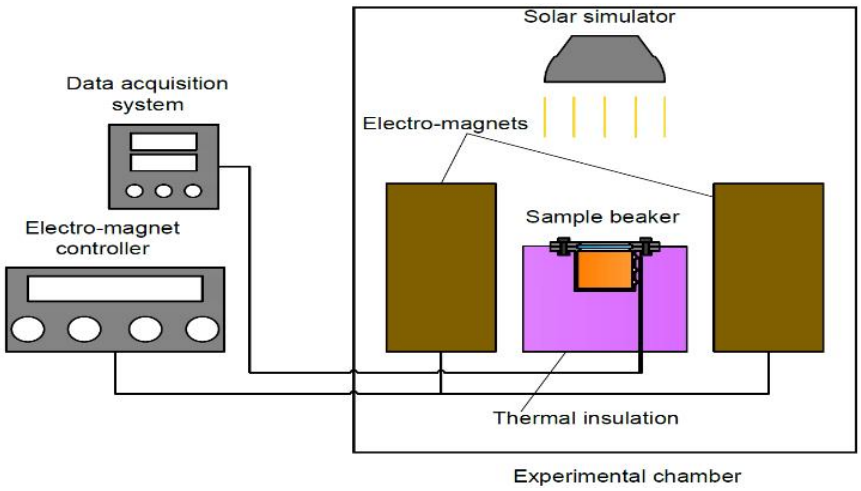


Fig. 2.9 Schematics of photo-thermal conversion experimental setup

Table 2.5 Accuracy of photo-thermal conversion measurement device

| Experiment | Model | Range | Accuracy |
|---|---|---|---|
| Photo-thermal conversion test | Thermo-couple (K-type) | -200 to 1300 | ±2.2°C |
| | Solar irradiation transmitter (CR-110) | 0-1500 W/m$^2$ | ±5% |


Fig. 2.10 Picture of (a) CR-110 Solar irradiation transmitter and K-type thermo couple

# Ⅲ. Results and discussion

## 3.1 Optical result of $Fe_3O_4$, MWCNT, and MWCNT/$Fe_3O_4$ hybrid nanofluid

The light transmittance experiment of the $Fe_3O_4$, MWCNT, and MWCNT/$Fe_3O_4$ hybrid nanofluids was carried out at room temperature of 25°C and the wavelength of the light spectrum ranged from 300 to 1100 nm.

Fig. 3.1 shows the variation of the optical transmittance of $Fe_3O_4$, MWCNT, and MWCNT/$Fe_3O_4$ hybrid nanofluid according to the concentration. The base fluid had a higher light transmittance compared to the $Fe_3O_4$, MWCNT, and MWCNT/$Fe_3O_4$ hybrid nanofluids. Due to the transparent color of water and ethylene glycol, the base fluid has a high light transmittance, the same as for water. As shown in results, the base fluid exhibits a smoothly constant transmittance at all wavelengths. In addition, the $Fe_3O_4$ nanofluid has a higher light transmittance than the MWCNT, MWCNT/$Fe_3O_4$ hybrid nanofluid. At higher concentrations of $Fe_3O_4$ nanofluid, the light transmittance of the $Fe_3O_4$ nanofluid was 0 at wavelengths 300-500 nm. Furthermore, the peak point of light transmittance in the $Fe_3O_4$ nanofluid was observed at the wavelength of 850 nm.

In Fig. 3.1(c), when the MWCNT nanoparticles were added to the $Fe_3O_4$ nanofluid, the color of the MWCNT/$Fe_3O_4$ nanofluid turned black. Due to the high light absorbance of MWCNT nanoparticles, the light absorbance of the MWCNT/$Fe_3O_4$ hybrid nanofluid was higher than the $Fe_3O_4$ nanofluid. The light transmittance of the MWCNT/$Fe_3O_4$ hybrid nanofluid shows a similar tendency to that in a study by Ham et al. [41]. The MWCNT/$Fe_3O_4$ hybrid nanofluid could

completely absorb all wavelengths except from weight concentration of 0.005wt%. Moreover, the light transmittance of the MWCNT/$Fe_3O_4$ hybrid nanofluid increased as the concentration of the MWCNT/$Fe_3O_4$ hybrid nanofluid decreased.

Fig. 3.2 shows the variation of the solar weighted absorption fraction of the $Fe_3O_4$ nanofluid with different weight concentration. As shown in Fig. 3.2, the solar weighted absorption fraction of the $Fe_3O_4$ nanofluid at a short penetration distance has a different trend according to the concentration of the nanofluid. The solar weighted absorption fraction of the $Fe_3O_4$ nanofluid was 1.0 at a penetration distance of 3 cm for concentrations greater than 0.05wt%. At a concentration of 0.2wt%, it was almost 1.0 at a penetration distance of 1 cm. However, the base fluid absorbed only 40% of the solar energy at a penetration distance of 5 cm. The solar weighted absorption fraction increased as the penetration distance increased. In the $Fe_3O_4$ nanofluid, the lowest solar weighted absorption fraction was observed at the $Fe_3O_4$ nanofluid concentration of 0.005wt%, but it showed a higher solar weighted absorption fraction than the base fluid.

The solar weighted absorption fraction of MWCNT nanofluid was presented in Fig. 3.3. In the case of MWCNT nanofluid, the solar weighted absorption fraction was not significantly dependent on the weight concentration of the MWCNT nanofluid. On the other hand, it is dependent on the penetration distance. The solar weighted absorption fraction of MWCNT nanofluid was 1.0 at a penetration distance of 1 cm, except for the 0.005wt% MWCNT nanofluid. Solar weighted absorption fraction of 0.005wt% nanofluid reached 0.9 at the penetration distance of 5 cm. Compared to the $Fe_3O_4$ nanofluid, all samples of MWCNT nanofluid absorbed significantly high solar energy at every penetration distance. This

phenomena can explained by cylinder shape and black color of MWCNT nanoparticle, that can efficiently scatter the light radiation.

Fig. 3.4 exhibits the solar weighted absorption fraction of MWCNT/$Fe_3O_4$ hybrid nanofluid with different weight concentrations. As a result, solar weighted absorption fraction of MWCNT/$Fe_3O_4$ hybrid nanofluid increased with the concentration and penetration distance. All samples of MWCNT/$Fe_3O_4$ hybrid nanofluid achieved higher solar weighted absorption fraction than $Fe_3O_4$ nanofluid, however it is also slightly lower than the single MWCNT nanofluid. The solar weighted absorption fraction of MWCNT/$Fe_3O_4$ hybrid nanofluid was 1.0 at a penetration distance of 1 cm, except for the 0.005wt% MWCNT/$Fe_3O_4$ hybrid nanofluid. The solar weighted absorption fraction of 0.005wt% reached about 0.85 at penetration distance of 5 cm.

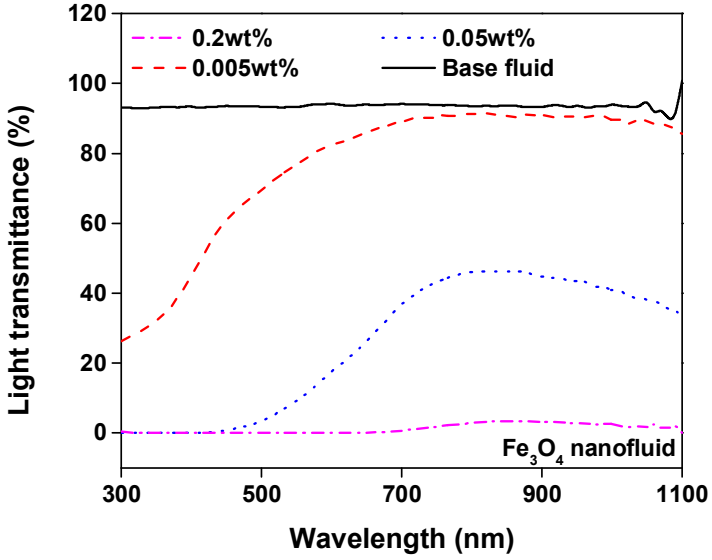


(a) $Fe_3O_4$ nanofluid

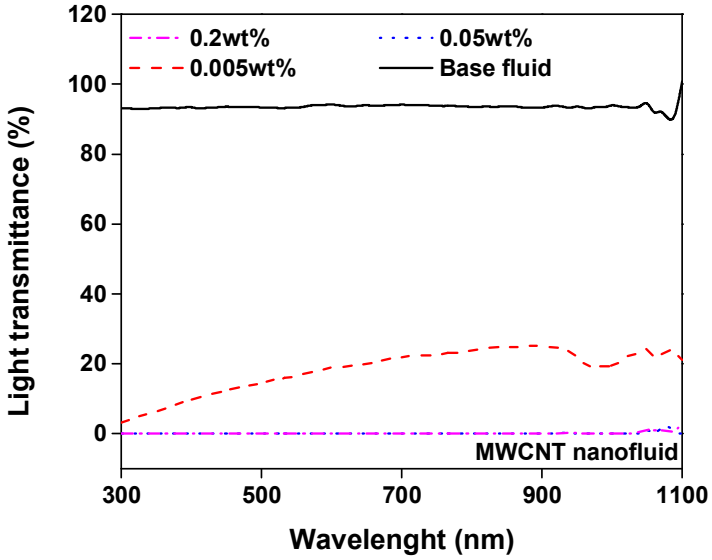


(b) MWCNT nanofluid

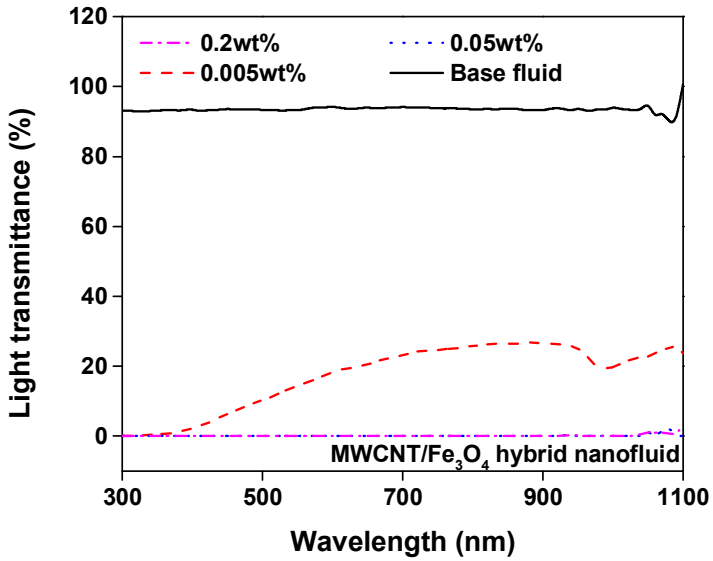


(c) MWCNT/$Fe_3O_4$ hybrid nanofluid

Fig. 3.1 Variation of optical transmittance of (a) $Fe_3O_4$, (b) MWCNT, and (c) MWCNT/$Fe_3O_4$ hybrid nanofluid

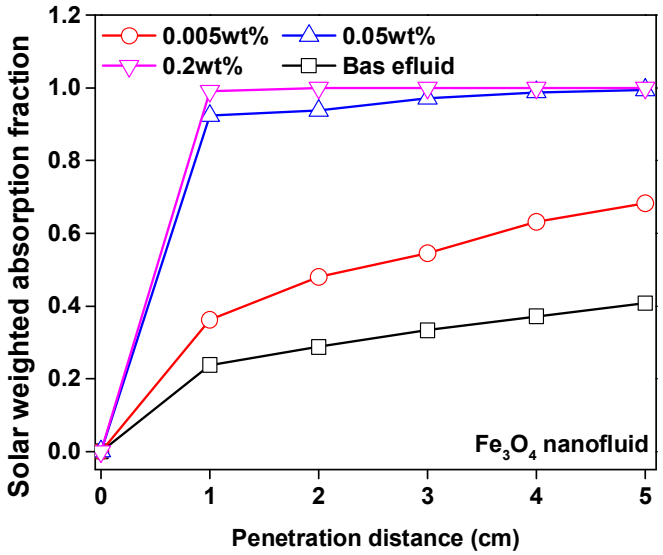


Fig. 3.2 Variation of the solar weighted absorption fraction of the $Fe_3O_4$ nanofluid with different weight concentration

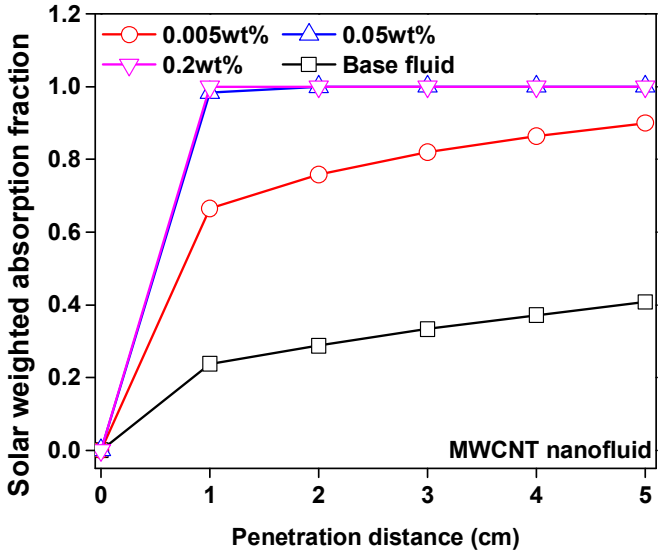


Fig. 3.3 Variation of the solar weighted absorption fraction of the MWCNT nanofluid with different weight concentration

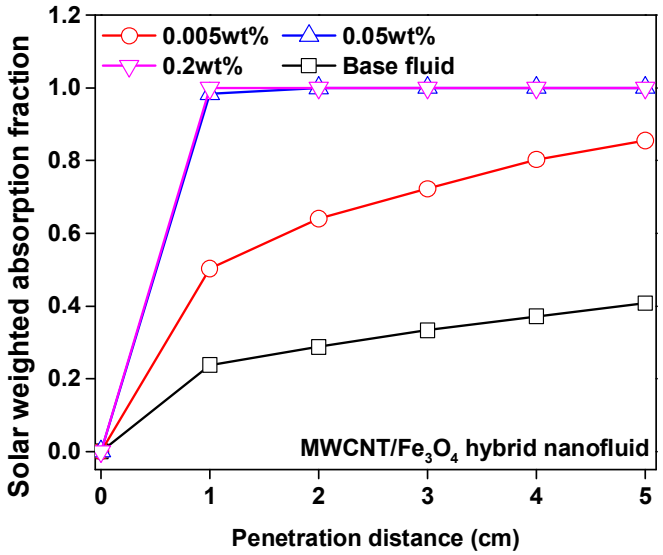


Fig 3.4 Variation of the solar weighted absorption fraction of the MWCNT/$Fe_3O_4$ hybrid nanofluid with different weight concentration

## 3.2 Thermal conductivity of $Fe_3O_4$, MWCNT, and MWCNT/$Fe_3O_4$ hybrid nanofluid

Fig. 3.5 presents the thermal conductivity variation of $Fe_3O_4$ nanofluid at different weight concentration without an external magnetic field. In this test, all samples of $Fe_3O_4$ nanofluid achieved greater thermal conductivity result than base fluid for all case. The increase in weight concentration and temperature of nanofluid leads to the thermal conductivity improvement in $Fe_3O_4$ nanofluid. The maximum thermal conductivity value of $Fe_3O_4$ nanofluid was 0.562 W/mK, which was observed at weight concentration and temperature of 0.2wt% and 50°C. In the Fig. 3.5, the thermal conductivity of $Fe_3O_4$ nanofluid exhibits the linear trend with temperature. Compared to the base fluid, the maximum thermal conductivity enhancement was 15.8%, which was observed at the at the weight concentration and temperature of 0.2wt% and 50°C. The increase of thermal conductivity in nanofluid can explained by augmentation of Brownian motion. Besides, it can be also explained by the increase of high specific heat transfer area between nanoparticles and fluid.

Fig. 3.6 shows the variation of thermal conductivity with temperature at different weight concentrations. In the Fig. 3.6, the thermal conductivity increase of MWCNT nanofluid was more notable at high concentration. The maximum value of thermal conductivity of MWCNT nanofluid was 0.58 W/mK, which was achieved at the concentration and temperature of 0.2wt% and 50°C. Compared to the base fluid, the maximum thermal conductivity enhancement of MWCNT

nanofluid was 19.5%, which was observed in weight concentration of 0.2wt% at the temperature of 50°C. As shown in Fig. 3.6, the thermal conductivity of MWCNT increases with the weight concentration and temperature. Compared to the thermal conductivity of $Fe_3O_4$ nanofluid and base fluid, the MWCNT nanofluid has a significantly high thermal conductivity under the same condition. Moreover, thermal conductivity of MWCNT shows the non-linear parallel trend as shown in Fig. 3.6.

Fig. 3.7 shows the variation of thermal conductivity of MWCNT/$Fe_3O_4$ nanofluid with temperature for different weight concentrations. The thermal conductivity of MWCNT/$Fe_3O_4$ hybrid nanofluid was significantly improved compared to that of $Fe_3O_4$ nanofluid. The maximum thermal conductivity of MWCNT/$Fe_3O_4$ hybrid nanofluid was 0.569 W/mK, which was observed in 0.2wt% MWCNT/$Fe_3O_4$ hybrid nanofluid at temperature of 50°C. This enhancement is caused by the effect of MWCNT nanoparticles. Even though, weight mixing ratio of hybrid nanofluid was fixed at 50:50 and number of MWCNT nanoparticles in hybrid nanofluid were so much greater than that of $Fe_3O_4$ nanoparticles because of their density differences. Due to the greater number of nanoparticles in hybrid nanofluid, each and every nanoparticles act as a thermal energy carrier that delivering the thermal energy to the each other effectively. Furthermore, it may can be assumed that because thermal energy transport distance between nanoparticles decreased, MWCNT nanoparticle was a relatively larger than $Fe_3O_4$ nanoparticle. According to the study of Baby et al [40], the decrease in thermal energy transport distance leads to the increase in the frequency of lattice vibration, thus thermal conductivity of nanofluid improves.

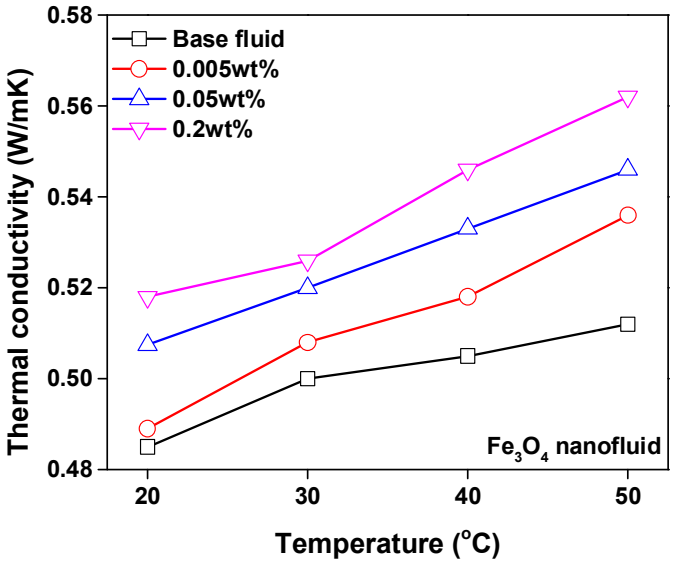


Fig. 3.5 Variation of thermal conductivity with temperature at different weight concentrations of $Fe_3O_4$ nanofluid

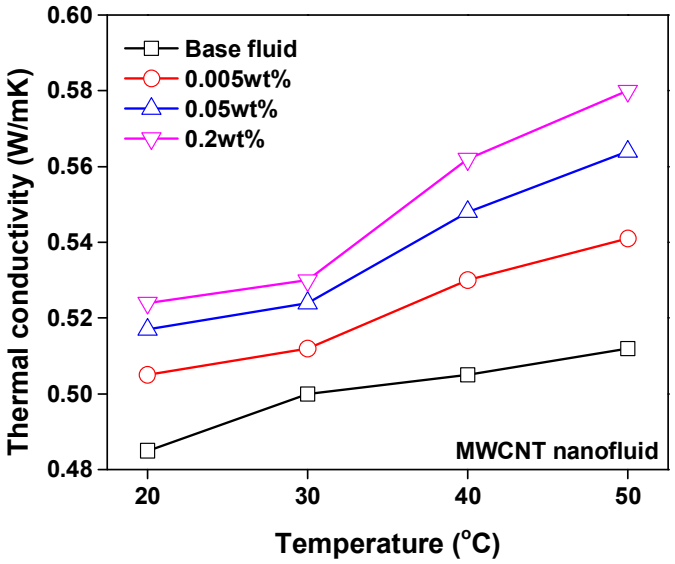


Fig. 3.6 Variation of thermal conductivity with temperature at different weight concentrations of MWCNT nanofluid

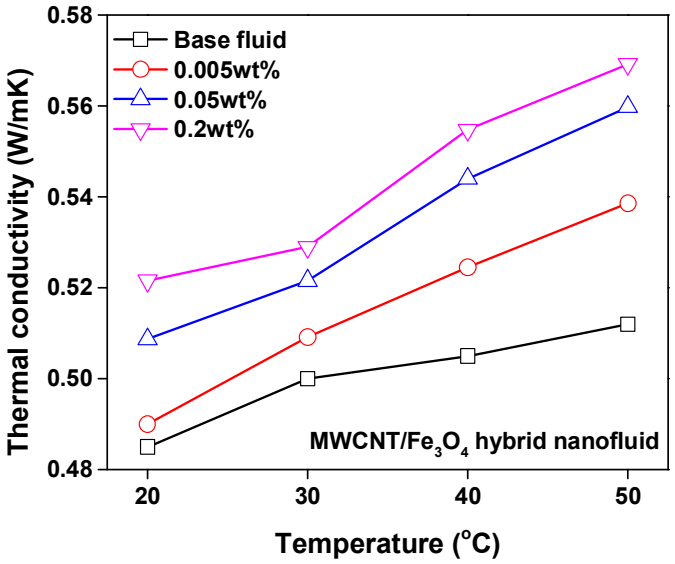


Fig. 3.7 Variation of thermal conductivity with temperature at different weight concentrations of MWCNT/$Fe_3O_4$ hybrid nanofluid

## 3.3 Thermal conductivity of $Fe_3O_4$ nanofluid under an external magnetic field

Fig. 3.8 shows the thermal conductivity variation of 0.005wt% $Fe_3O_4$ nanofluid under an external magnetic field. In the Fig. 3.8, the thermal conductivity of 0.005wt% $Fe_3O_4$ nanofluid increases with the increase of magnetic intensity and temperature. The thermal conductivity at 0.005wt% $Fe_3O_4$ nanofluid without a magnetic field was 0.489 and 0.536 W/mK at temperatures of 20°C and 50°C, respectively. The thermal conductivity of 0.005wt% $Fe_3O_4$ nanofluid under magnetic field intensity of 750 Gauss was 0.510 and 0.561 W/mK at temperatures of 20°C and 50°C, respectively. At a temperature of 50°C, the maximum increase in thermal conductivity with magnetic field was 15%, which was observed at a magnetic intensity of 750 Gauss, compared to that without magnetic field. Moreover, the $Fe_3O_4$ nanofluid shows a higher thermal conductivity than MWCNT nanofluid under external magnetic field at same weight concentration. The thermal conductivity 0.005wt% $Fe_3O_4$ nanofluid under different magnetic intensities was proportionally increased with the increase of magnetic intensity.

Fig. 3.9 presents the thermal conductivity variation of 0.05wt% $Fe_3O_4$ nanofluid under external magnetic field. The increase in thermal conductivity increase at 0.05wt% $Fe_3O_4$ nanofluid shows the linear relationship with temperature. The thermal conductivity of 0.05wt% $Fe_3O_4$ nanofluid without a magnetic field was 0.507 and 0.546 W/mK at temperatures of 20°C and 50°C, respectively. The thermal conductivity of 0.05wt% $Fe_3O_4$ nanofluid under an external magnetic field

intensity of 750 Gauss was 0.535 and 0.57 W/mK, at temperatures of 20°C and 50°C, respectively. At a temperature of 50°C, the maximum increase in thermal conductivity was 12%, which was observed at a magnetic intensity of 750 Gauss, compared to that without magnetic field. According to the thermal conductivity results of 0.05wt% $Fe_3O_4$ nanofluid, the magnetic and temperature effect on the increase of thermal conductivity was similar, compared to the 0.005wt% $Fe_3O_4$ nanofluid. As shown in Fig. 3.8, temperature effect on thermal conductivity increase of $Fe_3O_4$ nanofluid was relatively superior to that of the magnetic effect.

Fig. 3.10 shows the thermal conductivity variation of 0.2wt% $Fe_3O_4$ nanofluid under influence of external magnetic field. The increase of thermal conductivity at 0.2wt% $Fe_3O_4$ nanofluid presents the non-linear increase with temperature. The thermal conductivity at 0.2wt% $Fe_3O_4$ nanofluid without a magnetic field was 0.518 and 0.562 W/mK at temperatures of 20°C and 50°C, respectively. The thermal conductivity of 0.2wt% $Fe_3O_4$ nanofluid under an external magnetic field intensity of 750 Gauss was 0.551 and 0.583 W/mK at temperatures of 20°C and 50°C, respectively. At a temperature of 50°C, the maximum increase in thermal conductivity was 13%, which was observed at a magnetic intensity of 750 Gauss, compared to that without magnetic field. In addition, 0.2wt% $Fe_3O_4$ nanofluid has 20% enhanced thermal conductivity, compared to the base fluid, which was higher than that of MWCNT nanofluid at same weight concentration. Moreover, temperature effect on thermal conductivity of $Fe_3O_4$ nanofluid was dominant at high temperatures (40°C to 50°C); however, magnetic effect was superior at the lower temperatures. Compared to the other $Fe_3O_4$ samples under lower weight concentration, 0.2wt% $Fe_3O_4$ nanofluid presented mixed behaviour.

In the study of Philip et al. [42], when magnetic nanoparticles under influence

of external magnetic field, each and every nanoparticles behave as a single super magnetic domain, interacting with each others via dipole-dipole interaction. In a strong magnetic field, this dipolar interaction between magnetic nanoparticles creates chainlike structures in nanofluid. In the absence of a magnetic field, $Fe_3O_4$ nanoparticles move spontaneously, while in the presence of a magnetic field, $Fe_3O_4$ nanoparticles move in a single direction aligned with the direction of the magnetic field, which creating chainlike structure. This movement transports thermal energy more efficiently than random Brownian motion.

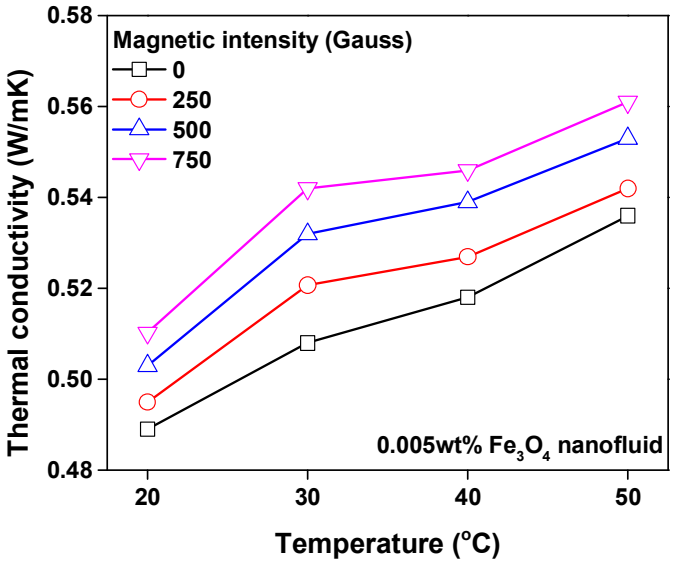


Fig. 3.8 Thermal conductivity variation of 0.005wt% $Fe_3O_4$ nanofluid under an external magnetic field

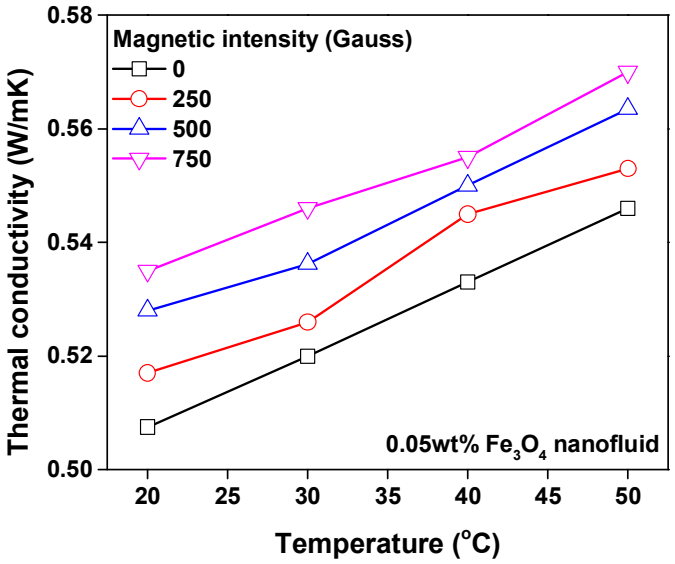


Fig. 3.9 Thermal conductivity variation of 0.05wt% $Fe_3O_4$ nanofluid under an external magnetic field

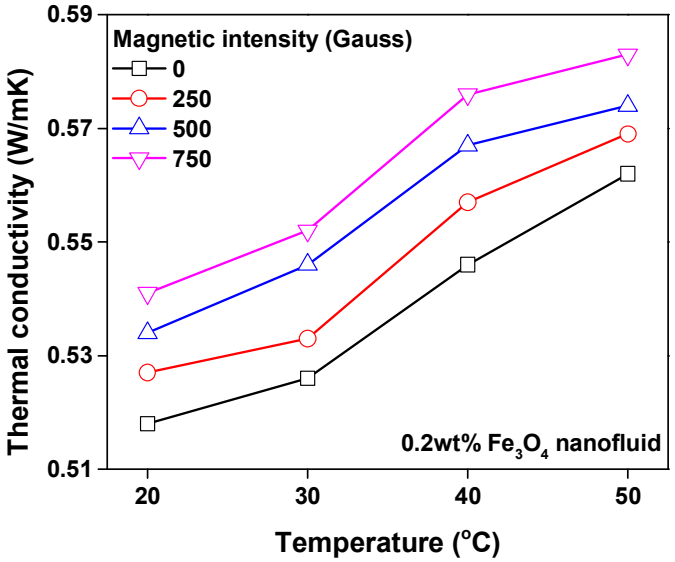


Fig. 3.10 Thermal conductivity variation of 0.2wt% $Fe_3O_4$ nanofluid under an external magnetic field

## 3.4 Thermal conductivity of MWCT/$Fe_3O_4$ hybrid nanofluid under an external magnetic field

Fig. 3.11 shows the variation of thermal conductivity of 0.005wt% MWCNT/$Fe_3O_4$ hybrid nanofluid under an external magnetic field. The thermal conductivity of 0.005wt% MWCNT/$Fe_3O_4$ hybrid nanofluid increases with the magnetic intensity and temperature. In the absence of magnetic field, the thermal conductivity of 0.005wt% hybrid nanofluid was 0.49 and 0.538 W/mK at the temperatures of 20°C and 50°C; however under 750 Gauss of magnetic intensity, its thermal conductivity was 0.516 and 0.565 W/mK, respectively. The maximum thermal conductivity enhancement of 0.005wt% MWCNT/$Fe_3O_4$ hybrid nanofluid was around 15%, which was presented under 750 Gauss magnetic intensity, compared to that without magnetic field. Additionally, the MWCNT/$Fe_3O_4$ nanofluid shows a higher thermal conductivity than MWCNT nanofluid under external magnetic field at same weight concentration. That means that adding MWCNT nanoparticles into $Fe_3O_4$ nanofluid bring significant thermal conductivity improvement under magnetic field, which even surpass the thermal conductivity of single MWCNT nanofluid.

Fig. 3.12 shows the variation of thermal conductivity of 0.05wt% MWCNT/$Fe_3O_4$ hybrid nanofluid under an external magnetic field. The thermal conductivity of 0.05wt% MWCNT/$Fe_3O_4$ hybrid nanofluid increases with the magnetic intensity and temperature. The thermal conductivity at 0.05wt% MWCNT/$Fe_3O_4$ nanofluid without a magnetic field was 0.508 and 0.559 W/mK at temperatures of 20°C and 50°C, respectively. The thermal conductivity of 0.005wt% MWCNT/$Fe_3O_4$ nanofluid under

an external magnetic field intensity of 750 Gauss was 0.54 and 0.583 W/mK at temperatures of 20°C and 50°C, respectively. At a temperature of 50°C, the maximum increase in thermal conductivity was 14%, which was observed at a magnetic intensity of 750 Gauss compared to that without magnetic field. Moreover, the MWCNT/$Fe_3O_4$ nanofluid shows higher thermal conductivity than MWCNT nanofluid under external magnetic field at same weight concentration. Moreover, the variation of thermal conductivity at 0.05wt% MWCNT/$Fe_3O_4$ hybrid nanofluid presents the same trend to that at 0.05wt% $Fe_3O_4$ nanofluid. Besides, the temperature and magnetic effect on thermal conductivity of nanofluids was nearly similar.

Fig. 3.13 shows the variation of thermal conductivity of 0.2wt% MWCNT/$Fe_3O_4$ hybrid nanofluid under an external magnetic field. The thermal conductivity of 0.2wt% MWCNT/$Fe_3O_4$ hybrid nanofluid increases with the magnetic intensity. The thermal conductivity at 0.2wt% MWCNT/$Fe_3O_4$ hybrid nanofluid without magnetic field was 0.521 and 0.569 W/mK at temperatures of 20°C and 50°C, respectively. The thermal conductivity of 0.005wt% MWCNT/$Fe_3O_4$ nanofluid under external magnetic field intensity of 750 Gauss was 0.547 and 0.5902 W/mK at temperatures of 20°C and 50°C, respectively. At a temperature of 50°C, the maximum increase in thermal conductivity was 13%, which was observed at a magnetic intensity of 750 Gauss compared to that without magnetic field. Moreover, the MWCNT/$Fe_3O_4$ nanofluid achieved higher thermal conductivity than MWCNT nanofluid under external magnetic field at same weight concentration. The 0.2wt% MWCNT/$Fe_3O_4$ hybrid nanofluid presents the logarithmic increase at high magnetic intensities; however, at low magnetic intensities it shows similar trend with that of $Fe_3O_4$ nanofluid at same weight concentration. In addition, it can be observed that the

thermal conductivity of the MWCNT/$Fe_3O_4$ hybrid nanofluid was relatively improved with increase of temperature and weight concentration of nanofluid, which means at the same magnetic intensities, hybrid nanofluid has higher thermal conductivity.

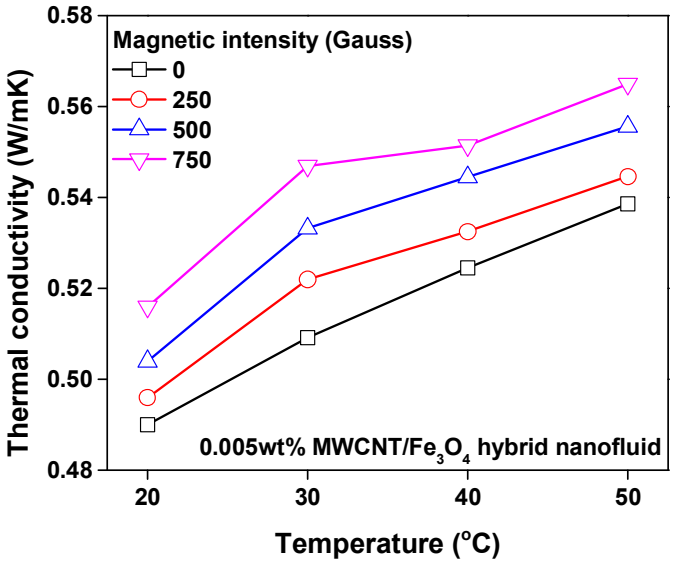


Fig. 3.11 Thermal conductivity variation of 0.005wt% MWCNT/$Fe_3O_4$ hybrid nanofluid under an external magnetic field

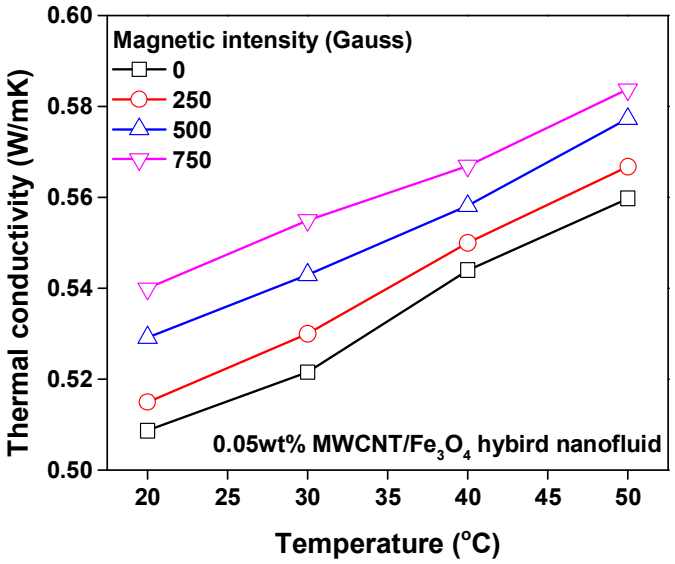


Fig. 3.12 Thermal conductivity variation of 0.05wt% MWCNT/$Fe_3O_4$ hybrid nanofluid under an external magnetic field

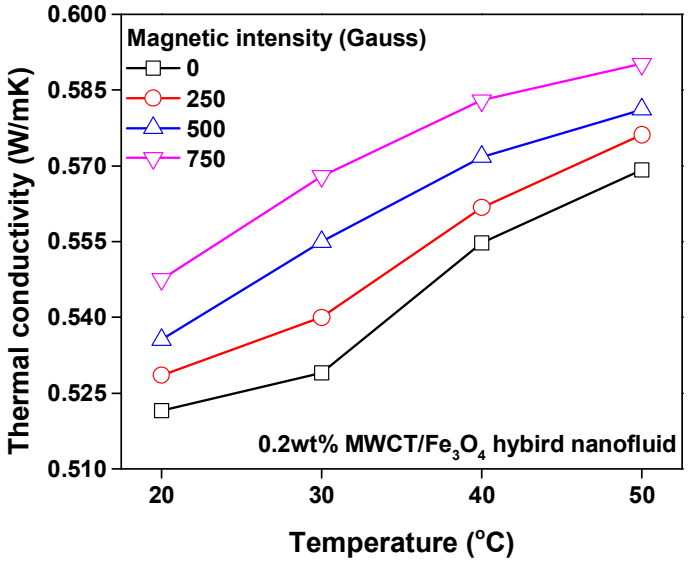


Fig. 3.13 Thermal conductivity variation of 0.2wt% MWCNT/$Fe_3O_4$ hybrid nanofluid under an external magnetic field

## 3.5 Photo-thermal conversion performance of $Fe_3O_4$, MWCNT, and MWCNT/$Fe_3O_4$ hybrid nanofluid

Fig. 3.14 shows the temperature variation of the $Fe_3O_4$ nanofluid according to the time during the photo-thermal conversion experiment. The average ambient temperatures was 20°C. The $Fe_3O_4$ nanofluid was heated by Halogen solar lamp with an average solar irradiation of 560 W/$m^2$ for 1 h. The temperature of $Fe_3O_4$ nanofluid increased as the experimental time passed. The photo-thermal conversion ability increased proportionally to the increase of weight concentration of $Fe_3O_4$ nanofluid. In the case of the base fluid, the temperature increased by 11°C after 1 h. The maximum temperature increment of the $Fe_3O_4$ nanofluid was 22.7°C which was observed at the concentration of 0.2wt%, which was about 2 times higher than that of base fluid.

Fig. 3.15 shows the variation of temperature with the time for MWCNT nanofluid, the maximum temperature increment of the MWCNT nanofluid was 26.36°C, observed at the MWCNT weight concentration of 0.2wt% after 1 h. Additionally, the temperature of the MWCNT nanofluid and base fluid increased with the increase of time and weight concentration. At the same concentration of 0.2wt%, after 1 h, the final temperatures of $Fe_3O_4$ and MWCNT nanofluid was 43.6°C and 47.2°C, respectively. This phenomenon can be explained by the difference between the thermal conductivity and solar weighted absorption fraction of $Fe_3O_4$ and MWCNT nanoparticles. Moreover, MWCNT nanofluid exhibited the superior performance on the solar weighted absorption fraction

compared to the $Fe_3O_4$ nanofluid.

Fig. 3.16 presents the photo-thermal variation of MWCNT/$Fe_3O_4$ hybrid nanofluid with time for various weight concentrations. The temperature of MWCNT/$Fe_3O_4$ hybrid nanofluid increases with the weight concentration of nanofluid and operating time. The maximum temperature of MWCNT/$Fe_3O_4$ hybrid nanofluid was 45°C at the weight concentration of 2wt% after 1 hour. In the Fig. 3.16, adding the MWCNT nanoparticles into the $Fe_3O_4$ nanofluid increased the photo-thermal conversion performance of $Fe_3O_4$ nanofluid. Temperatures of MWCNT/$Fe_3O_4$ nanofluid were slightly higher than those of $Fe_3O_4$ nanofluid; however those were lower than the MWCNT nanofluid at the same weight concentration. This is because that the thermal conductivity and solar weighted absorption fraction of MWCNT/$Fe_3O_4$ hybrid nanofluid is lower than those of MWCNT nanofluid, while higher than those of $Fe_3O_4$ nanofluid under absence of magnetic field. At the same weight concentration of 0.2wt%, final temperature of MWCNT/$Fe_3O_4$ hybrid nanofluid was 45°C, which was 1.46°C higher than $Fe_3O_4$ nanofluid, while 2.14°C lower than MWCNT nanofluid.

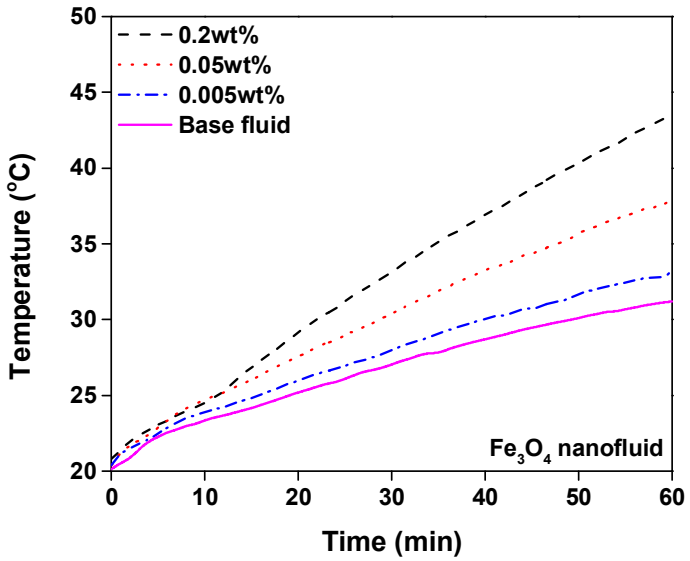


Fig. 3.14 Variation of temperature with the time for $Fe_3O_4$ nanofluid

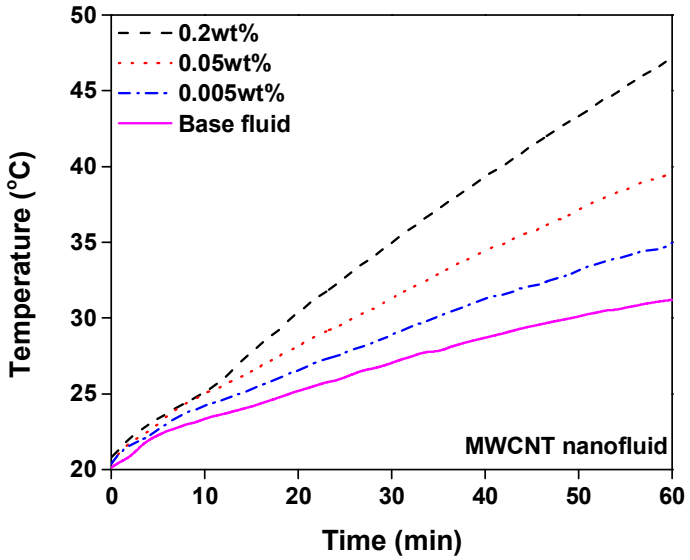


Fig. 3.15 Variation of temperature with the time for MWCNT nanofluid

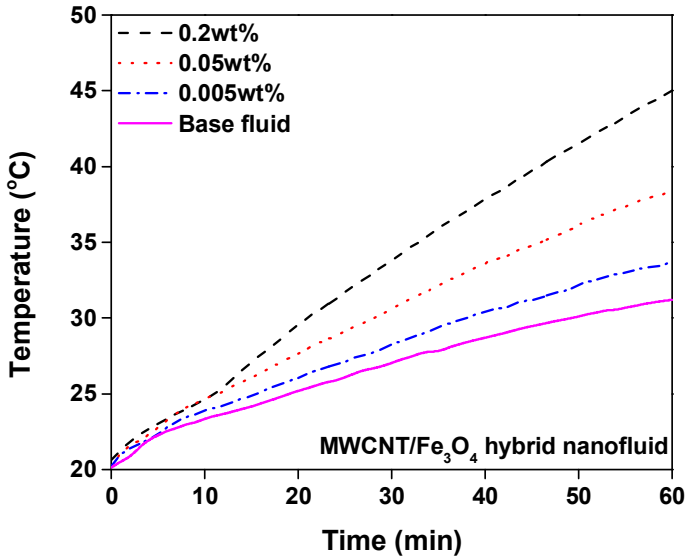


Fig. 3.16 Variation of temperature with the time for MWCNT/$Fe_3O_4$ hybrid nanofluid

## 3.6 Magnetic effect on photo-thermal conversion performance of MWCNT/$Fe_3O_4$ hybrid nanofluid

Fig. 3.17 shows the variation photo-thermal conversion performance at 0.2wt% MWCNT/$Fe_3O_4$ hybrid nanofluid under different magnetic intensities. The photo-thermal conversion performance of 2wt% MWCNT/$Fe_3O_4$ hybrid nanofluid improves with increase of operating time and magnetic intensity. The maximum temperature in the absence and presence of magnetic field was 45°C (without magnetic field) and 60°C (magnetic field with an intensity of 750 Gauss), respectively. This phenomenon also can be explained by the chainlike structure of $Fe_3O_4$ nanoparticles under magnetic field. The temperature increase in photo-thermal conversion performance of 0.2wt% MWCNT/$Fe_3O_4$ hybrid nanofluid in absence of magnetic field was from 20°C to 45°C, which was about 118% temperature increase. Moreover, the temperature increase in photo-thermal conversion experiment of 0.2wt% MWCNT/$Fe_3O_4$ hybrid nanofluid in presence of 750 Gauss magnetic intensity was from 20°C to 60°C, which was about 190% temperature increase. Furthermore, 0.2wt% MWCNT/$Fe_3O_4$ hybrid nanofluid presented more significant temperature increase in photo-thermal conversion test than MWCNT nanofluid at same weight concentration under 750 Gauss magnetic intensity.

This phenomenon also can be explained by the improved specific surface area and chainlike structure of $Fe_3O_4$ nanoparticles under a magnetic field as shown in Fig 3.18. In the case of MWCNT/$Fe_3O_4$ hybrid nanofluid under magnetic field,

MWCNT nanoparticles flow with the magnetic field direction and $Fe_3O_4$ nanoparticles because $Fe_3O_4$ nanoparticles attached to the MWCNT nanoparticle and act as transporter of MWCNT nanoparticle, as shown in 2.4(c). This chainlike structure can be proved by viscosity increase in $Fe_3O_4$ nanofluid under an external magnetic field. Experimental study of Wan et al. [43] shows that viscosity of $Fe_3O_4$ nanofluid was surprisingly increased, which was 175% enhancement in 0.1vol% $Fe_3O_4$ nanofluid under 550 Gauss magnetic intensity. This viscosity increase of $Fe_3O_4$ nanofluid [44,45] can be show that $Fe_3O_4$ nanoparticles create structure in nanofluid under external magnetic field that can affect the visosity of the fluid.

Fig. 3.19 shows the photo-thermal conversion efficiency of 0.2wt% MWCNT/$Fe_3O_4$ nanofluid under various magnetic intensities. The photo-thermal conversion efficiency increased with the magnetic intensity; while it decreased with operating time. The maximum photo-thermal conversion efficiency with and without the magnetic field was 54% and 65%, at the magnetic intensity of 750 Gauss, and 0.2wt% MWCNT/$Fe_3O_4$ nanofluid after 20 min operating time. Thereafter, due to the increase of fluid temperature, photo-thermal conversion efficiency decreased by around 4% every 20 min.

Fig. 3.20 presents the total stored energy of the 0.2wt% MWCNT/$Fe_3O_4$ hybrid nanofluid with different magnetic intensities during the photo-thermal conversion experiment for 1 h. The graph indicates that the increase of the magnetic intensity leads that increase of total stored energy in the 0.2wt% MWCNT/$Fe_3O_4$ hybrid nanofluid significantly. The maximum total stored energy was 15005 kJ, shown for the magnetic intensity of 750 Gauss at concentration of 0.2wt%. Compared to the absence of the magnetic field, the maximum enhancement of

the total stored energy was 61.51% at the magnetic intensity of 750 Gauss. Due to this thermal property enhancement, the MWCNT/$Fe_3O_4$ hybrid nanofluid can increase the thermal efficiency in the heat transfer or thermal system when it is used under magnetic field.

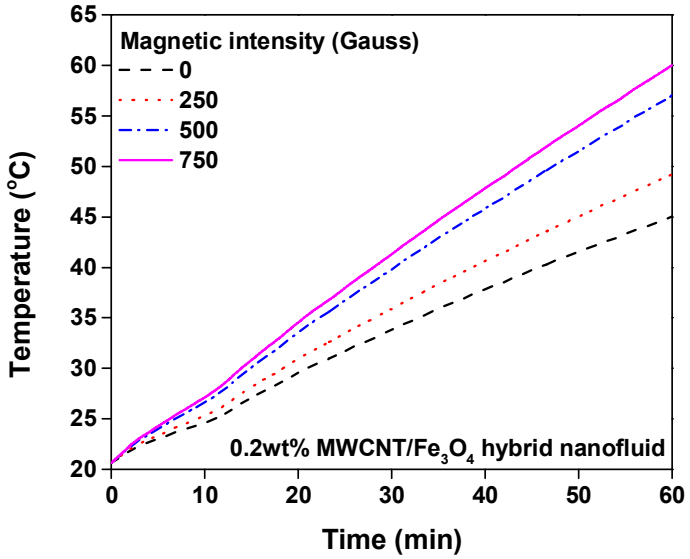


Fig. 3.17 Variation of temperature with the time for 0.2wt% MWCNT/$Fe_3O_4$ hybrid nanofluid under different magnetic intensity

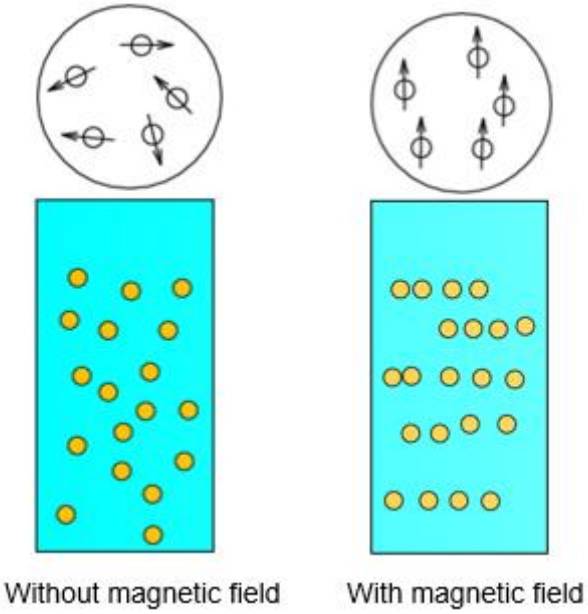


Fig. 3.18 Schematic of $Fe_3O_4$ nanoparticles under magnetic field

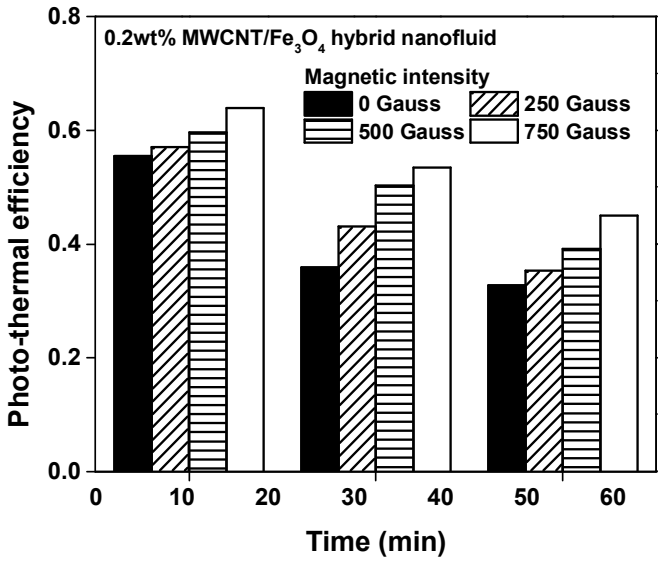


Fig. 3.19 Photo-thermal conversion efficiency of 0.2wt% MWCNT/$Fe_3O_4$ hybrid nanofluid under different magnetic intensities

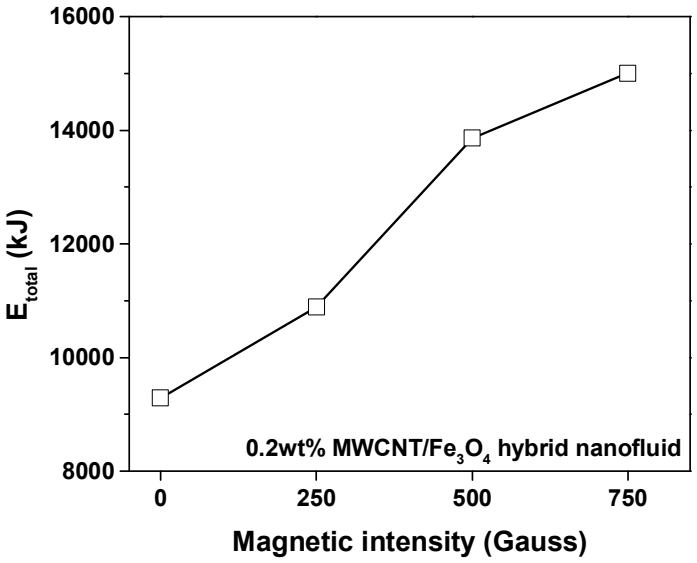


Fig. 3.20 Total stored energy in 0.2wt% MWCNT/$Fe_3O_4$ hybrid nanofluid during the heating process with different magnetic intensities

# IV. Conclusion

The thermal conductivity and photo-thermal conversion performance of $Fe_3O_4$, MWCNT, and MWCNT/$Fe_3O_4$ hybrid nanofluid were experimentally investigated under various magnetic intensity (250, 500, 750 Gauss). The weight concentration of nanofluid changed by 0.005wt%, 0.05wt%, and 0.2wt%, and the weight mixing ratio MWCNT/$Fe_3O_4$ hybrid nanoparticle was fixed at 50:50. According to the investigations in this study, the following results are obtained:

[1] The solar weighted absorption fraction of the $Fe_3O_4$ nanofluid is enhanced by an increase in the concentration and penetration distance. Furthermore, adding MWCNT nanoparticle into $Fe_3O_4$ nanofluid increase solar weighted absorption fraction of $Fe_3O_4$ nanofluid.

[2] The thermal conductivity of the $Fe_3O_4$, MWCNT, and MWCNT/$Fe_3O_4$ hybrid nanofluid was enhanced by an increase in the concentration and temperature. The maximum thermal conductivity of $Fe_3O_4$, MWCNT, and MWCNT/$Fe_3O_4$ hybrid nanofluid were 0.562, 0.58, and 0.569 W/mK at concentration and temperature of 0.2wt% and 50°C without an external magnetic field, respectively, while the thermal conductivity of $Fe_3O_4$ and MWCNT/$Fe_3O_4$ hybrid nanofluid increased with the increases of magnetic field intensity. The maximum thermal conductivity of $Fe_3O_4$ and MWCNT/$Fe_3O_4$ hybrid nanofluid was 0.583 W/mK and 0.59 W/mK under magnetic intensity of 750 Gauss, respectively.

[3] According to the photo-thermal conversion experiment, after 1 h, the temperatures of the $Fe_3O_4$, MWCNT and MWCNT/$Fe_3O_4$ hybrid nanofluid reached to 43.5°C, 45.03°C, and 47.1°C, respectively, at the same concentration of 0.2wt% without the magnetic field, while the final temperature of 0.2wt% MWCNT/$Fe_3O_4$ hybrid nanofluid was 60°C under magnetic intensity of 750 Gauss. This could be explained by the ability of the photo-thermal conversion enhanced by adding a small amount of MWCNT nanoparticles to the $Fe_3O_4$ nanofluid. The MWCNT/$Fe_3O_4$ hybrid nanofluid, containing the MWCNT nanoparticles, had a better photo-thermal conversion efficiency.

This thermal properties improvement of $Fe_3O_4$ and MWCNT/$Fe_3O_4$ nanofluid under can be explained by chainlike structure of magnetic nanoparticle in magnetic field. Under influence of external magnetic field, each and every magnetic nanoparticles behave as a single super magnetic domain, interacting with each others via dipole-dipole interaction. In a strong magnetic field, this dipolar interaction between magnetic nanoparticles creates chainlike structures in nanofluid. In the absence of a magnetic field, $Fe_3O_4$ nanoparticles move spontaneously; but in the presence of a magnetic field, $Fe_3O_4$ nanoparticles move in a single direction aligned with the direction of the magnetic field, creating this chainlike structure. This movement transports thermal energy more efficiently than random Brownian motion.

# REFERENCE

[1] Eastman, J.A.; Choi, U.S.; Li, S.; Thompson, L.J.; Lee, S. Enhanced thermal conductivity through the development of nanofluids. 1996

[2] K. Maaz. Silver nanoparticles: Fabrication, Characterization and Applications.

[3] W. Guo, G. Li, Y. Zheng, C. Dong, Measurement of the thermal conductivity of $SiO_2$ nanofluid with an optimized transient hot wire method, J. Thermochemical Acta. 661 (2018) 84-97.

[4] N. Kumar, S.S. Sonawane, Experimental study of thermal conductivity and convective heat transfer enhancement using CuO and $TiO_2$ nanoparticles, J. International Communications in Heat and Mass transfer. 76 (2016) 98-107.

[5] B. Wei, C. Zou, X. Li, Experimental investigation on stability and thermal conductivity of diathermic oil based $TiO_2$ nanofluid, J. International Journal of Heat and Mass transfer. 104 (2017) 537-543.

[6] M. Vakili, M. Karami, S. Delfani, S. Khosrojerdi, K. Kalhor, Experimental investigation and modeling of thermal conductivity of CuO-water/EG nanofluid by FFBP-ANN and multiple regressions, J. Thermal Analysis and Calorimetry. 129 (2017) 629-637.

[7] M. H. Ahmadi, A. Mirlohi, M. A.Nazari, Roghayeh Ghasempour, A review of

thermal conductivity of various nanofluid, J. Molecular Liquids. 265 (2018) 181-188.

[8] M. I. Pryazhnikov, A. V. Minakov, V. Ya. Rudyak, D. V. Guzei, Thermal conductivity measurements of nanofluid, J. Heat and Mass Transfer. 104 (2017) 1275-1282.

[9] H. Kim, J. Kim, H. Cho. Review of Thermal Performance and Efficiency in Evacuated Tube Solar Collector with Various Nanofluid. Int. J. Air-Conditioning and Refrigeration. 25 (2017)

[10] T. B. Gorji, A. A. Ranjbar, A numerical and experimental investigation on the performance of a low-flux direct absorption solar collector (DASC) using graphite, magnetite and silver nanofluid. J. Solar Energy. 135 (2016) 493-505

[11]A. Asadi, M. Asadi, A. Rezaniakolaei, L. A. Rosendahl, M. Afrand, S. Wongwises. Heat transfer efficiency of $Al_2O_3$-MWCNT/thermal oil hybrid nanofluid as a cooling fluid in thermal and energy management applications: An experimental and theoretical investigation. Int. J. Heat and Mass Transfer. 117(2018) 474-486.

[12]S. Suresha, K.P. Venkitaraja, P. Selvakumar, M. Chandrasekar. Synthesis of $Al_2O_3$-Cu/water hybrid nanofluid using two step method and its thermo physical properties. J. Colloids and Surfaces A: Physicochem. Eng. Aspects.

388 (2011) 41-48

[13] A. Parsian, M. Akbari. New experimental correlation for the thermal conductivity of ethylene glycol containing $Al_2O_3$-Cu hybrid nanoparticles. J. Therm Anal Calor. (2017)

[14] A. S. Dalkılıç, G. Yalçın, B. O. Küçükyıldırım, S. Öztuna, A. A. Eker, C Jumpholkul, S. Nakkaew, S. Wongwises. Experimental study on the thermal conductivity of water-based CNT-$SiO_2$ hybrid nanofluid. Int. J. Communications in Heat and Mass transfer. 99 (2018) 18-25

[15] A. Akhgar, D. Toghraie. An experimental study on the stability and thermal conductivity of water-ethylene glycol/$TiO_2$-MWCNTs hybrid nanofluid: Developing a new correlation. J. Powder Technology. 338 (2018) 806-818

[16] P. V. Trinh, N. N. Anh, N. T. Hong, P. N. Hong ,P. N. Minh, B. H. Thang. Experimental study on the thermal conductivity of ethylene glycol-based nanofluid containing Gr-CNT hybrid material. J. Molecular Liquids. 269 (2018) 344-353

[17] S. Aberoumand, A. Jafarimoghaddam. Tungsten (III) oxide ($WO_3$) - Silver/transformer oil hybrid nanofluid: Preparation, stability, thermal conductivity and dielectric strength. J. Alexandria Engineering. 57 (2018) 169-174.

[18] M. H. Esfe, S. Esfandeh, M. K. Amiri, M. Afrand. A novel applicable experimental study on the thermal behavior of SWCNTs(60%)-MgO(40%)/EG hybrid nanofluid by focusing on the thermal conductivity. J. Powder Technology. 342 (2019) 998-1007

[19] M. Karami. Experimental investigation of first and second laws in a direct absorption solar collector using hybrid $Fe_3O_4/SiO_2$ nanofluid. J. Thermal Analysis and Calorimetry. 136 (2016) 661-671

[20] V. M. Midhun, A. M. Sajeeb. Improving Efficiency of DASC by adding $CeO_2$/CuO hybrid nanoparticles in water. Int. J. Nanoscience. 3 (2017)

[21] V. Bhalla, V. Khullar, H. Tyagi. Experimental investigation of photo-thermal analysis of blended nanoparticles ($Al_2O_3/Co_3O_4$) for direct absorption solar thermal collector. J. Renewable Energy. 123 (2018) 616-626

[22] M. S. Liu, M. C.C Lin, T. Huang, Chi-Chuan Wang. Enhancement of thermal conductivity with carbon nanotube for nanofluids. J. Int. Communications in Heat and Mass Transfer 32 (2005) 1202 - 1210

[23] J. Qu, M. Tian, X. Han, R. Zhang, Q. Wang, Photo-thermal conversion characteristics of MWCNT-$H_2O$ nanofluids for direct solar thermal energy absorption applications, J. Applied Thermal Engineering, 124 (2017) 486-493

[24] B. Abreu, B. Lamas, A. Fonseca, Experimental characterization of convective heat transfer with MWCNT based nanofluids under laminar flow conditions, J. Heat Mass Transfer, 50 (2013)

[25] M. Soltanimehr, M. Afrand. Thermal conductivity enhancement of COOH-functionalized MWCNTs/ethylene glycol-water nanofluid for application in heating and cooling systems. J. Applied Thermal Engineering. 105 (2016) 716-723

[26] A. Karimi, M. Goharkhah, M. Ashjaee, M. b. Shafii. Thermal conductivity of $Fe_2O_3$ and $Fe_3O_4$ Magnetic nanofluids under the influence of magnetic field. J. Int. Thermophysics. 598 (2015) 59-67

[27] M. Hajiyan, S. Ebadi, S. Mahmud, M. Biglarbegian, H. Abdullah. Experimental investigation of the effect of an external magnetic field on the thermal conductivity and viscosity of $Fe_3O_4$-glycerol. J. Thermal analysis and Calorimetry. 135 (2018) 1451-1464
-018-7531

[28] L. Sha, Y. Ju, H. Zhang, The influence of the magnetic field on the convective heat transfer characteristics of $Fe_3O_4$/water nanofluids, J. Applied Thermal Engineering, 126 (2017) 108-116

[29] M. Amani, M. Ameri, A. Kasaeian, Investigating the convection heat transfer of $Fe_3O_4$ nanofluid in a porous metal foam tube under constant magnetic field, J. Experimental Thermal and Fluid Science, 82 (2017)

439-449

[30] L. S. Sundar, M. T. Naik, K. V. Sharma, M. K. Singh, T. Ch. Reddy, Experimental investigation of forced convection heat transfer and friction factor in a tube with $Fe_3O_4$ magnetic nanofluid, J. Experimental Thermal and Fluid Science, 37 (2012) 65-71

[31] L. Shi, Y. He, Y. Huang, B. Jiang, Recyclable $Fe_3O_4$@CNT nanoparticles for hig-efficiency solar vapor generation, J. Energy Conversion and Management, 149 (2017) 401-408

[32] L. S. Sundar, M. K. Singh, Antonio C.M. Sousa. Enhanced heat transfer and friction factor of MWCNT-$Fe_3O_4$/water hybrid nanofluid. Int. J. Communications in Heat and Mass Transfer. 52 (2014) 73-83.

[33] S. S. Harandi, A. Karimipour, M. Afrand, M. Akbari, A. D'Orazio. An experimental study on thermal conductivity of F-MWCNTs-$Fe_3O_4$/EG hybrid nanofluid: Effects of temperature and concentration. Int. J. Communications in Heat and Mass Transfer. 76 (2016) 171-177.

[34] R. Mohebbi, M. Izadi, A. A. Delouei, H. Sajjadi. Effect of MWCNT-$Fe_3O_4$/water hybrid nanofluid on the thermal performance of ribbed channel with apart sections of heating and cooling. J. Thermal Analysis and Calorimetry. 135 (2019) 3029-3042

[35] L. Shi, Y. He , Y. Hu, X. Wang. Thermophysical properties of $Fe_3O_4$@CNT nanofluid and controllable heat transfer performance under magnetic field. J. Energy Conversion and Management. 177 (2018) 249-257

[36] M. Gupta, V. Singh, S. Kumar, S. Kumar, N. Delbaghi, Z. Said. Up to date review on the synthesis and thermophysical properties of hybrid nanofluid. J. Cleaner Production. 190 (2018) 169-192

[37] J. A. R. Babu, K. K. Kumar, S. S. Rao. State-of-art review on hybrid nanofluids. J. Renewable and Sustainable Energy Reviews. 77 (2017) 551-565

[38] J. R. Howell, R. Siegel, M. P. Menguc, Thermal Radiation Heat Transfer, 5th edition, (2011)

[39] Carolina L.L. Beicker, M. Amjad, Enio P. B. Filhoa, Dongsheng Wen. Experimental study of photothermal conversion using gold/water and MWCNT/water nanofluids. J. Solar Energy Materials and Solar Cells. 188 (2018) 51-65

[40] J. Ham, Y. Shin, H. Cho. Optical-thermal properties of an MWCNT/EG nanofluid intended as the working fluid in a direct absorption solar collector. J. High Temperatures - High Pressures. 48 (2019) 121-193

[41] T.T. Baby, R. Sundara. Synthesis and Transport of Metal Oxide Decorated

Graphene Dispersed Nanofluid. J. Physical Chemistry. 115 (2011) 8527-8533

[42] Philip. J, Shilma. P.D, Baldev Ra, (2007), 'Enhancement of thermal conductivity in magnetite based nanofluid due to chainlike structures', J. Applied Physics Letters, Vol 91

[43] Wan. L, Wang. Y, Yan. X, Wang. X, Feng. B.Investigation on viscosity of $Fe_3O_4$ nanofluid under magnetic field. J. International Communications in Heat and Mass Transfer, Vol 72 (2016) 23-28

[44] Pouranfard. A, Rahimi. M. R.Experimental Investigations on the Viscosity of Magnetic Nanofluids under the Influence of Temperature, Volume Fractions of Nanoparticles and External Magnetic Field. J. Applied Fluid Mechanics. Vol 9 (2016) 93-697

[45] Hajiyan M, Ebadi. S, Mahmud. S, Biglarbegian. M, Abdullah. H,Experimental investigation of the effect of an external magnetic field on the thermal conductivity and viscosity of $Fe_3O_4$-glycerol. J. Thermal Analysis and Calorimetry